

NIST Technical Note NIST TN 2288

NIST Eave and Vent Experiments (EaVE) EaVEs Phase A: Test Plan

Christopher U. Brown
Alexander Maranghides
Shonali Nazare
Giovanni Di Cristina
D. Michelle Bailey
Lucy Fox
Eric Link
Selvarajah Ramesh
Xareni Monroy
J. Houston Miller
Erin E. McCaughey
Monica M. Flores

This publication is available free of charge from: https://doi.org/10.6028/NIST.TN.2288



NIST Technical Note NIST TN 2288

NIST Eave and Vent Experiments (EaVE) EaVEs Phase A: Test Plan

Christopher U. Brown
Alexander Maranghides
Shonali Nazare
Giovanni Di Cristina
Lucy Fox
Eric Link
Selvarajah Ramesh
Fire Research Division
Engineering Laboratory

D. Michelle Bailey Chemical Sciences Division Material Measurement Laboratory J. Houston Miller Erin E. McCaughey Monica M. Flores Department of Chemistry, George Washington University, Washington, DC 20052, USA

Xareni Monroy Insurance Institute for Businesses & Home Safety

This publication is available free of charge from: https://doi.org/10.6028/NIST.TN.2288

May 2024



U.S. Department of Commerce Gina M. Raimondo, Secretary

National Institute of Standards and Technology Laurie E. Locascio, NIST Director and Under Secretary of Commerce for Standards and Technology Certain equipment, instruments, software, or materials, commercial or non-commercial, are identified in this paper in order to specify the experimental procedure adequately. Such identification does not imply recommendation or endorsement of any product or service by NIST, nor does it imply that the materials or equipment identified are necessarily the best available for the purpose.

The policy of the National Institute of Standards and Technology is to use metric units in all its published materials. Because this report is intended for the U.S. building construction industry, which uses inch-pound units, it is more practical and less confusing to use inch-pound units, in some cases, rather than metric units. However, in most cases, units are presented in both metric and the inch-pound system.

Another policy of the National Institute of Standards and Technology is to include statements of uncertainty with all NIST measurements. In this document, however, some measurements of authors outside of NIST are presented, for which uncertainties were not reported and are unknown.

NIST Technical Series Policies

<u>Copyright, Use, and Licensing Statements</u> <u>NIST Technical Series Publication Identifier Syntax</u>

Publication History

Approved by the NIST Editorial Review Board on 2024-05-15

How to Cite this NIST Technical Series Publication

Brown CU, Maranghides A, Nazare S, Di Cristina G, Bailey DM, Fox L, Link E, Ramesh S, Monroy X, Miller JH, McCaughey EE, Flores MM (2024) NIST Eave and Vent Experiments (EaVE) EaVEs Phase A: Test Plan. (National Institute of Standards and Technology, Gaithersburg, MD), NIST Technical Note (TN) NIST TN 2288. https://doi.org/10.6028/NIST.TN.2288

Author ORCID iDs

Christopher U. Brown: 0000-0002-0426-2249 Alexander Maranghides: 0000-0002-3545-2475

Shonali Nazare: 0000-0002-0407-5849

Giovanni Di Cristina Torres: 0000-0002-0799-3418

D. Michelle Bailey: 0000-0001-6273-3830

Lucy Fox: 0009-0004-7725-708X Eric Link: 0000-0002-7784-5023

Selvarajah Ramesh: 0000-0002-9525-6767 Xareni Monroy: 0000-0002-2240-4079 J. Houston Miller: 0000-0002-6686-1976 Erin E. McCaughey: 0009-0004-3757-6238 Monica M. Flores: 0009-0003-1101-5961

Contact Information

christopher.brown@nist.gov

Abstract

This test plan documents experiments that are part of ongoing research to assess structure-to-structure fire spread in the Wildland-Urban Interface (WUI). Previous indoor and outdoor full-scale experiments were conducted with varying distance between sheds and the exterior wall of a primary residence. The current experiments were planned to understand the failure of the eave vents used in previous experiments. The objective of these full-scale experiments is to characterize the performance of representative eave vents exposed to fire from the source structure. Metal sheds of varying sizes and fuel loads (wood cribs) will be burned under the 20 MW exhaust hood in the National Fire Research Laboratory (NFRL) at the National Institute of Standards and Technology (NIST) at varying structure separation distances (SSDs) from the target structure. The target structure includes an assembly of an exterior wall, a roof, and an eave vent. A range of measurements will be taken during the experiments including heat release rate, heat flux, temperature, gas flow velocity, and gas species concentration using open-path absorption spectroscopy. Video and infrared cameras will record the experiments. A separate NIST Technical Note will report the results of these experiments.

Keywords

absorption spectroscopy; attic vents; auxiliary structures; community fire spread; eaves; fire; gas flow velocity; gas species concentration; heat flux measurements; heat release rate; modeling; open-path absorption spectroscopy; sheds; temperature measurements; vents; wildland fire; wildland-urban interface

Table of Contents

1.	Overvi	ew	1
2.	Objecti	ves	3
3.	Eave V	ent Experiments	.4
	3.1 Exp	eriment Configuration	. 4
	3.1.1	Target Structure – Roof, Wall, Eaves	. 4
	3.1.2	Source Structure - Shed	. 6
	3.1.3	Source Structure - Fuel Loading	. 7
	3.1.4	Fire Ignition	. 9
	3.1.5	Data Acquisition	. 9
	3.2	Technical Issues	14
	3.3	Source-Structure-Only Experiment Configuration	15
	3.3.1	Objective	15
	3.3.2	Instrumentation	15
	3.3.3	Preliminary Experiment Matrix	15
	3.4	Eave Vent Experiment Matrix	17
	3.4.1	Objective	17
	3.4.2	Experiment Parameters	17
	3.4.3	Experiment Decision Matrix	18
	3.5 Mo	deling	19
4.	Uncert	ainty of Measurements	20
5.	Data M	anagement	22
6.	Refere	nces	23
Αį	pendix	A – Target Structure Design and Specifications	25
Αį	pendix	B – Source Structures	34
Αį	pendix	C - Elevated Platform Design	35
Αį	pendix	D – Experiment SOP	41
Αį	pendix	E - Modeling Details	44
Li	st of Ta	bles	
Ta	ble 1. G	alvanized Steel Shed Specifications (1 ft = 0.0305 m, 1 lb = 0.453 kg)	7
		nstrumentation locations related to the target structure where the origin is the bottom	
		the wall	
		rimary experiment parameters (1 ft = 0.0305 m).	
Ta	ble 4. E	xperiment sequence based on flowchart	19

Table 5. Simulations cases varying dimension in different directions45
Table 6. Schematic of the attic rear for each tested opening configuration46
Table 7. Mean temperature in the central bay (B1), the adjacent bay (B2), and within the adjacent rafters (R1 and R2). Standard deviation is indicated within parentheses48
List of Figures
Fig. 1. Full-scale shed experiments without wind1
Fig. 2. A full-scale outdoor shed experiment with applied wind field2
Fig. 3. Plan view of the experiment layout under the 20 MW exhaust hood in the NFRL (figure not to scale)4
Fig. 4. The target structure with roof, wall and eave plenum and source structure (figure not to scale).
Fig. 5. The eave vent plenum view from the attic side of the vent (figure not to scale)6
Fig. 6. The low or high fuel load configuration for the Closet shed with two or four 1-A cribs, respectively (figure not to scale)8
Fig. 7. The low fuel load configuration for the Very Small shed with four 1-A cribs (figure not to scale).8
Fig. 8. The low, medium, and high fuel load configuration for the Narrow shed with either two, four, or six 1-A cribs, respectively (figure not to scale)8
Fig. 9. Location of the 6 heat flux gauges in the eaves. Gauges 1, 3 and 5 face the source structure from the eave bays while gauges 2, 4 and 6 face the source structure from the underside of the roof overhang (figure not to scale)9
Fig. 10. The heat flux gauge, bi-directional probe, and thermocouple locations on the front face (exposed side) of the target structure (figure not to scale)11
Fig. 11. The positions of the 5 video cameras (black) including the video camera position at the face of the target structure, and one IR camera (white) (figure not to scale)
Fig. 12. Unscaled mockup of laser instrument incorporated into the target structure set up. The target structure is shown in the center with laser launch and collection platforms on either side. The laser stands are anchored to the floor supporting the elevated platforms approximately 3.7 m (12 ft) above ground level (figure not to scale)
Fig. 13. Horizontal and vertical distances between laser path A through the eaves and path B behind the eave vent14
Fig. 14. Laser path B behind the eave vent passes just under the rafters to pass through concentrated gases (figure not to scale; 1 in = 2.54 cm)
Fig. 15. Plan view of the preliminary experiment layout with the sheds facing the heat flux gauges (figure not to scale)
Fig. 16. Conditional flowchart for experiment matrix. Vent failures will be repeated a total of three times
Fig. 17. EaVE Target Structure (dimensions in inches; 1 in. = 2.54 cm)25
Fig. 18. Target wall construction details with roof overhang (figure not to scale)31

Fig. 19. Eave height for a single-story family residence [2]32
Fig. 20. Load and boundary conditions of laser support platform35
Fig. 21. Elevated platform attachment to the laser instrument setup (dimensions in inches; 1 in. = 2.54 cm)
Fig. 22. Elevated platform attachment to the top of the support columns (dimensions in inches; 1 in. = 2.54 cm)
Fig. 23. Elevated platform attachment to the two columns and column attachment to the floor (front view; dimensions in inches; 1 in. = 2.54 cm)39
Fig. 24. Top view of the elevated platform and columns to the north and south of the target structure with the roof peak centered under the hood40
Fig. 25. Simulation set up considering (a) heat source 1.44 m above the floor and (b) heat source at floor level
Fig. 26. Location of temperature and oxygen fraction measurements beneath the eave45
Fig. 27. Mean temperature and oxygen fraction for various opening configurations for simulation case SxSySz
Fig. 28. Volume location where averaged oxygen fraction was computed during the simulations47
Fig. 29. Time histories of volume-averaged oxygen fractions across (a) the eave area and (b) the attic.
Fig. 30. Result for the simulation case SxSySz with and without attic, (a) wind speed and (b) gas temperature, both measured 2 cm inside the eave vent opening

1. Overview

The experiments outlined in this report are part of a series of experiments related to structure-to-structure fire spread in Wildland-Urban Interface (WUI) communities. The overall project is divided into three phases assessing radiant and convective heat exposures from different size fire sources. The fire sources in Phase 1 are small storage sheds (<11 m² (120 ft²)) commonly used on residential properties.

Fire sources for Phase 1 experiments include storage sheds, ranging in size from 1.39 m² to 24.8 m² (15 ft² to 267 ft²). A series of indoor experiments without wind was conducted as part of the NIST Indoor Structure Separation Experiments (NISSE) series [1,2] (Fig. 1). Full-scale shed burn experiments were conducted at the National Fire Research Laboratory (NFRL) at the National Institute of Standards and Technology (NIST) and at the Insurance Institute for Business & Home Safety (IBHS) with various types of source structures used to generate typical radiative and convective heat exposures to target structures that simulated a residential exterior wall. The spacing between the source and target structures was varied to identify safe structure separation distances (SSD). Heat release rate, mass loss rate, and heat flux were also measured.

The results of these experiments suggested that the radiant heat and flames from both combustible wooden sheds and noncombustible steel sheds could ignite the target structure. While the noncombustible steel shed did not burn, the flames from the burning contents of the steel shed could ignite the target structure. Fire spread on the roof and within the attic space was evident even with low fuel loadings and in the absence of wind.



Fig. 1. Full-scale shed experiments without wind.

Following the NISSE experiments, Phase 1 experiments continued with the NIST Outdoor Structure Separation Experiments (NOSSE) [3,4] (Fig. 2). The primary objective of these full-scale outdoor experiments was to study the effects of wind on fire spread and to identify safe SSDs needed to prevent fire spread in WUI communities. These experiments were conducted in an artificially generated wind field. Varying sizes of source structures (sheds) with varying wood crib loadings (source of fuel) were used to generate typical radiative and convective heat exposures to the target structure: an assembly of a single-story residential building exterior wall with a window and roof.

This series resulted in quantification of the minimum SSD between a shed and a primary residence under the experimental conditions. The minimum SSD was identified as 3 m (10 ft) for both combustible and noncombustible sheds with floor area less than 2.4 m^2 (26 ft²) in scenarios with a fire-hardened target structure. For sheds with floor area between 2.4 m^2 (26 ft²) and 5.9 m^2 (64 ft²), the minimum SSD was found to be 4.6 m (15 ft). Because the local winds during a WUI fire are unpredictable, SSD should be the same in all directions.



Fig. 2. A full-scale outdoor shed experiment with applied wind field.

While this test plan describes experiments related to sheds (Phase 1), the focus of this series is on assessing the failure of eave vents observed during the previous indoor and outdoor experiments. This experiment series will be referred to as "EAVES Phase A." Following the completion of EAVES Phase A, additional experiments will assess the performance of other eave vents with different operating mechanisms. The final series will be EAVES Phase C experiments that will aim to develop recommendations to revise the ASTM E2886 test method [5] for eave vents or to propose a new test method.

2. Objectives

Based on the results of the previous Phase 1 experiments [2, 4], this next set of experiments are planned to understand the failure of the eave vents used during the NISSE and NOSSE experiments. These experiments also use sheds, but the specific focus of the experiments is the failure of the eave vent rather than ignition of the target structure and identification of SSD.

The objective of these experiments is to characterize the performance of a California Building Standards Code Chapter 7A (Chapter 7A) Wildfire Flame and Ember Resistant (WUI) vent with an intumescent coating exposed to flames from the burning source structure. Noncombustible steel sheds of varying sizes and fuel loads (wood cribs) will be burned under the 20 MW exhaust hood in the NFRL at different SSDs from the target structure. The target structure will be similar to previously used target structures (exterior wall approximately 4.9 m (16 ft) long by 4 m (13 ft) high and roof assembly with typical construction materials as per Chapter 7A [6]) used during the NISSE series except without a window. A series of preliminary shed-only experiments will be conducted to burn the wood cribs as fuel with no target structure in place.

The objective of these experiments will be to answer the following questions:

- 1.1 What is the lower boundary thermal exposure for vent failures?
- 1.2 Does the vent work in the activation temperature regime specified by the ASTM E 2886 test method [5]?
- 1.3 When the vents fail to perform as expected, why are the failures occurring? Two hypotheses we examine are, a) the intumescent coating does not activate, and b) the intumescent coating gets blown away because of the high plume velocity of smoke and air, which will be better understood after these experiments. The later effect is not considered in the current ASTM E 2886 test method but is present in WUI fires.

3. Eave Vent Experiments

These eave vent experiments are designed to better understand the performance of the vents as a function of fire exposure. These vents were used previously during the shed burn experiments with [4] and without wind [2].

3.1 Experiment Configuration

These eave vent experiments will be conducted indoors without wind at NIST's NFRL under the 20 MW hood. The experiment layout is shown in Fig. 3 below. The peak of the target structure roof will be centered under the hood.

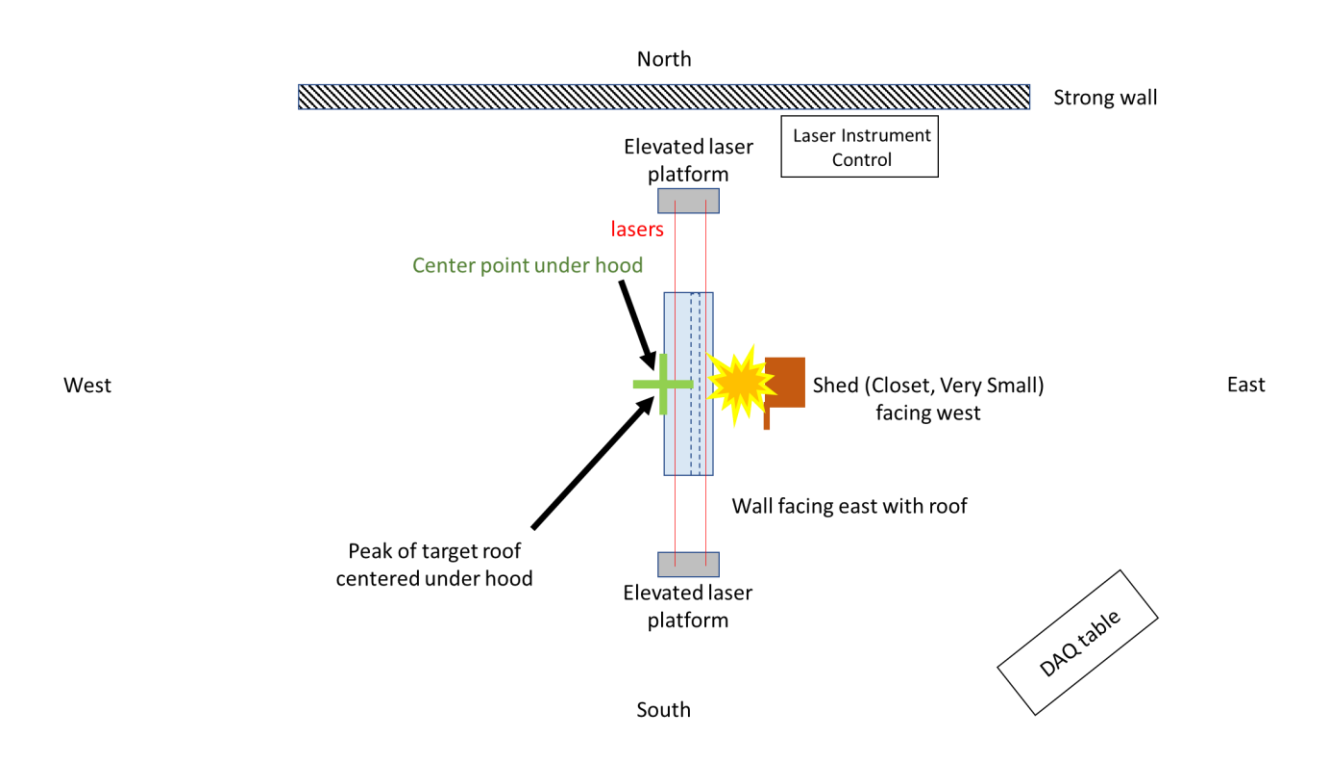


Fig. 3. Plan view of the experiment layout under the 20 MW exhaust hood in the NFRL (figure not to scale).

3.1.1 Target Structure – Roof, Wall, Eaves

The proposed target structure is similar to those constructed previously [2] to represent the façade of a single-story residence (Appendix A and Fig. 18). The target structure will be composed of a roof-wall assembly with a vented attic. The target structure will be oriented north and south under the exhaust hood with the exterior side of the structure facing east, and the opening of the source shed facing either west (Fig. 3) or south. A weighing platform to measure mass loss used during previous experiments to estimate the heat release rate will not be used because only steel sheds will be used in these experiments.

Roof

The roof will be built in compliance with Chapter 7A requirements [6]. The roof will have asphalt shingles, be at an approximate pitch of 5:12 with an open eave configuration and will measure approximately 1.8 m (6 ft) from aluminum gutter to roof peak. The wood rafters will measure approximately 61 cm (24 in) on center so that each rafter bay is approximately 57.2 cm (22.5 in). The roof overhang from the wall will be 46 cm (18 in). Metal drip edge flashing will be installed.

Wall

The target wall will be constructed with nominal 2-in by 4-in wood studs, approximately 41 cm (16 in) on center (o.c.). Each stud bay is therefore approximately 36.8 cm (14.5 in) wide between the studs. The exterior layer of the wall (cladding) will be fiber cement siding with a nominal thickness of 8 mm (5/16 in), the middle layer will be noncombustible drywall with a nominal thickness of 16 mm (5/8 in), and an interior oriented strand board (OSB) layer with a nominal thickness of 11 mm (7/16 in) attached to the wood studs. Fiberglass insulation approximately 9 cm (3.5 in) thick will be inserted between the wood framing studs. Drywall will also be used on the interior side of the studs (Appendix A, Fig. 17) to encapsulate the insulation.

The target wall will be approximately 4 m (13 ft) tall and 4.9 m (16 ft) wide. The height of the eaves will be approximately 4 m (13 ft) from the ground. The overall height of the target structure will be approximately 4.6 m (15 ft) from the ground to the peak of the roof (Fig. 4). Unlike previous experiments, there will be no window in the wall.

Eaves

A WUI eave vent with an intumescent coating that was observed to not perform as expected during the previous NISSE and NOSSE experiments will be used for each experiment in the center rafter bay. Vent dimensions are approximately 19 cm by 56 cm (7.5 in by 22 in). Fire-resistant caulking will be applied around the vent from the exterior side, as is standard installation practice. The selected WUI eave vent conforms to Chapter 7A [6] and ASTM E2886 [5] and is commonly used in residential construction in WUI areas.

The eave vent plenum will be constructed in the central rafter bay of the target structure, similar to the one used during the NISSE series. A negative pressure exhaust fan will not be used nor cotton batting on the false floor of the plenum. The plenum will have drywall along the sides that will extend approximately 0.6 m (2 ft) back from the vent on the attic side. Drywall will form the plenum false floor (Fig. 5).

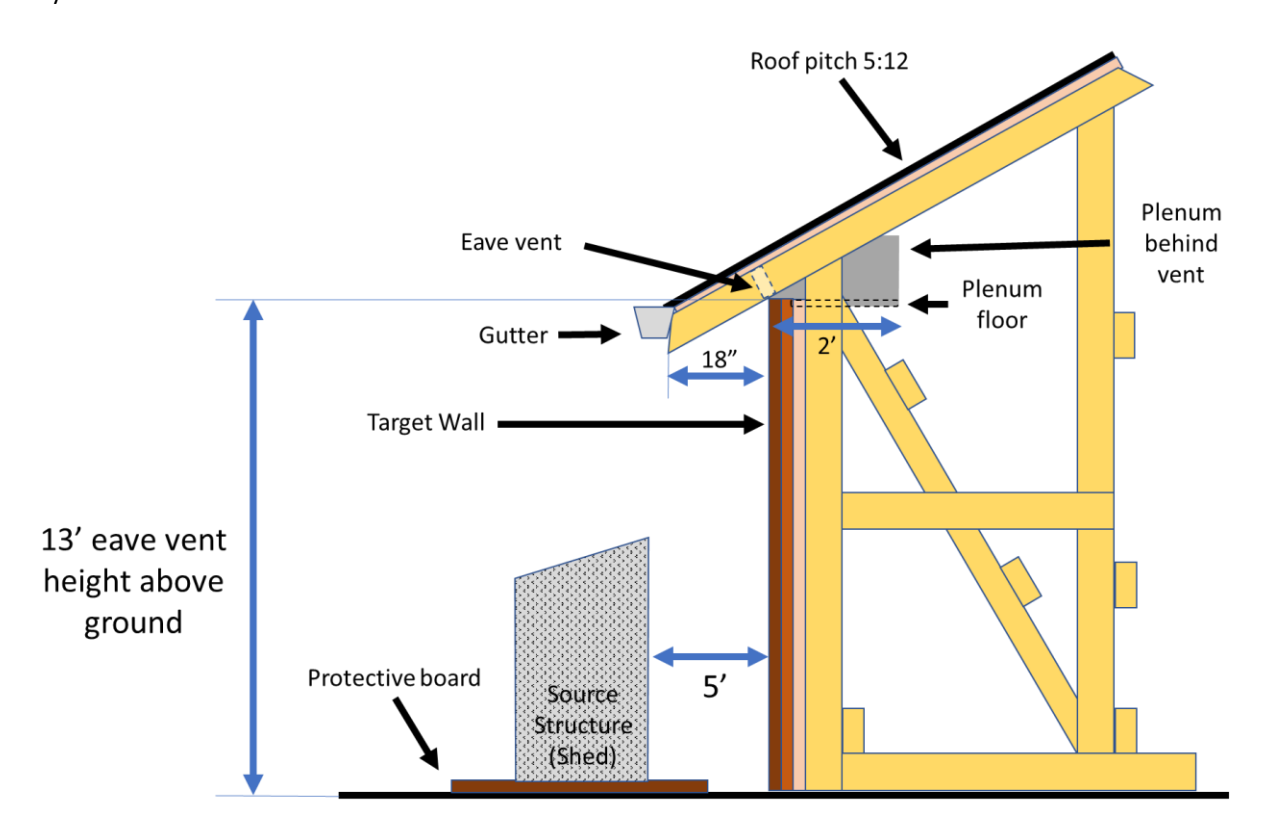


Fig. 4. The target structure with roof, wall and eave plenum and source structure (figure not to scale).

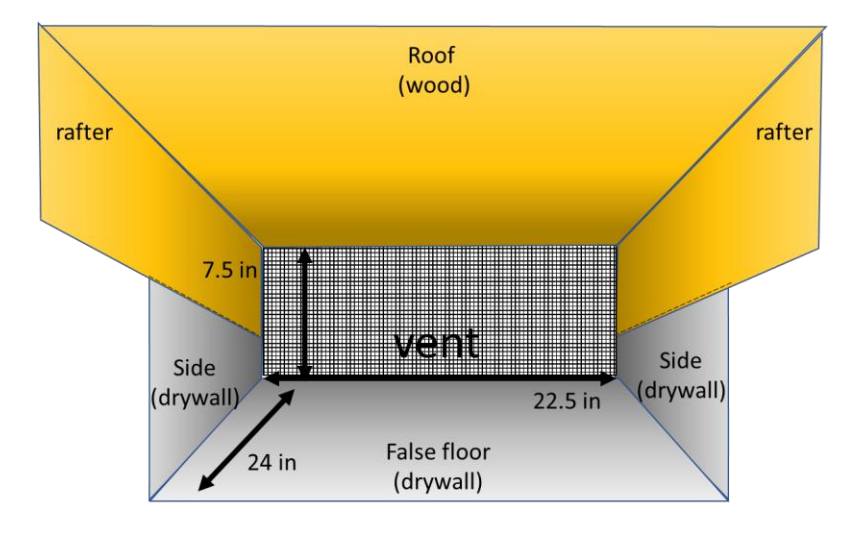


Fig. 5. The eave vent plenum view from the attic side of the vent (figure not to scale).

3.1.2 Source Structure - Shed

For these experiments, the source structures will be new galvanized steel sheds of three styles: Closet (C) (intended for storing trash cans), traditional sheds (single door, noted as Very Small (VS) in previous experiments [1,2]), and a Narrow Lean-to shed (N) (a double door shed

designed to fit against an exterior wall of a residence) (Table 1) (Appendix B). Based on previous experiments, the metal sheds produce a flame jet that will be aimed towards the eave vent. All sheds will have a completely open-door configuration for these experiments. If the amount of fire exposure from the source structure to eave vent needs to be adjusted, the shed door may be partially closed.

The Closet and Very Small sheds will be positioned so that their doorway is facing the target structure (0-degree orientation) with a 1.5 m (5 ft) SSD. The Narrow sheds will be positioned against the target structure with a 0 m SSD, but the shed door will be facing 90 degrees to the target structure. The Narrow shed has not been tested previously and therefore will be part of the preliminary experiments to determine the location where the Narrow shed should be positioned so that the flame jet is aligned with the eave vent.

Galvanized Steel Shed Styles	Examples	Size D x W x H (ft)	Capacity (ft³)	Door W x H (ft) / Area (ft²)	Weight (lb)	Notes
Closet (C)		3 x 6 x 4	66	4.8 x 4 / 19	77	Double door and lid Vents: No
Very Small (VS)		5 x 6 x 6	141	2.6 x 5 / 13.5	107	Single door, Vents: 4 gable vents
Narrow Lean-To (N)		6.5 x 4 x 5	154	3 x 5 / 16	125	Double door, Vents: No

Table 1. Galvanized Steel Shed Specifications (1 ft = 0.0305 m, 1 lb = 0.453 kg).

3.1.3 Source Structure - Fuel Loading

Pine wood cribs based on the UL 711 design [7] will be used as fuel for these experiments. Only size 1-A cribs will be used with 12 layers of 6 members each with approximate dimensions of 38 mm x 38 mm x 500 mm (1.5 in x 1.5 in x 20 in) and 54 mm (2.1 in) between 2 members. The overall dimensions of the cribs are approximately 500 mm x 500 mm x 456 mm (19.7 in x 19.7 in x 18 in). The average mass of a 1-A crib is 19.36 kg \pm 0.8 kg (uncertainty is \pm 2 σ , where σ is the standard deviation). The moisture content of the cribs will vary between 5 % and 7 %.

Based on the amount of fire exposure to the target structure, the number of cribs to be used in each shed will vary. It is anticipated that for the Closet sheds a fuel loading of either 2 cribs (low) or 4 cribs (high) will be used (Fig. 6). For the Very Small sheds either 4 cribs (low) or 6 cribs

(high) will be used (Fig. 7). For the Narrow sheds, 2 cribs will be used for the low fuel, 4 cribs for the medium fuel, and 6 cribs for the high fuel (Fig. 8).

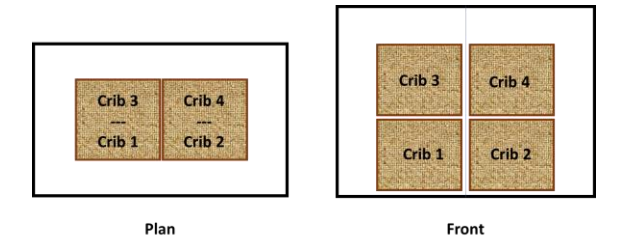


Fig. 6. The low or high fuel load configuration for the Closet shed with two or four 1-A cribs, respectively (figure not to scale).

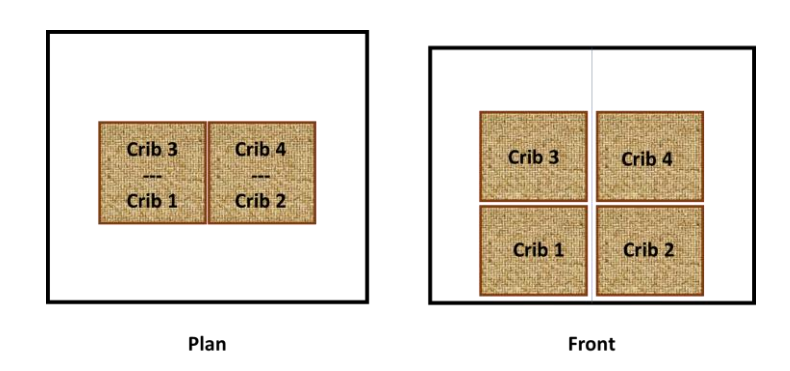


Fig. 7. The low fuel load configuration for the Very Small shed with four 1-A cribs (figure not to scale).

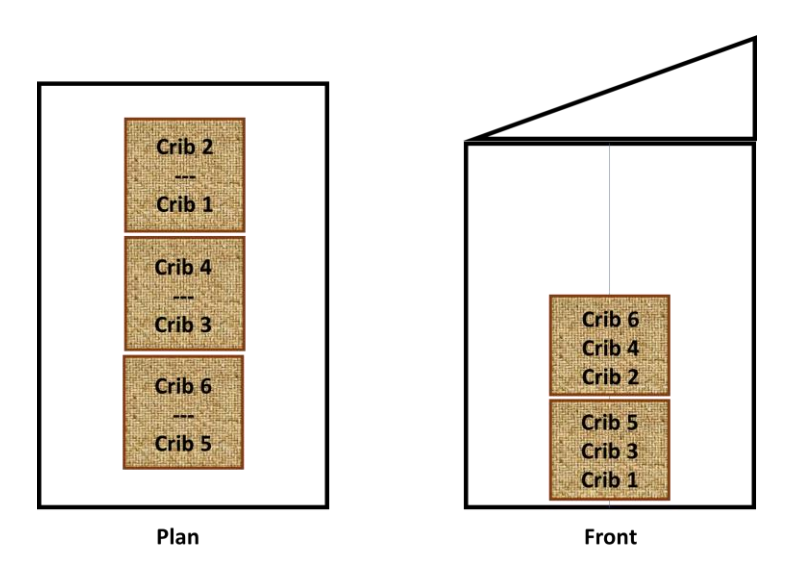


Fig. 8. The low, medium, and high fuel load configuration for the Narrow shed with either two, four, or six 1-A cribs, respectively (figure not to scale).

3.1.4 Fire Ignition

The wood cribs inside the source structures (metal sheds) will be ignited using 300 mL of heptane in an aluminum pan of nominal dimensions 90 mm \times 130 mm \times 30 mm (7.5 in \times 5 in \times 1.25 in). This method of wood crib ignition is known to be reproducible [8]. The heptane in the aluminum pan will be ignited using a hand-held propane tank and wand.

3.1.5 Data Acquisition

Measurements will include heat flux, temperature, fire-induced gas flow velocity, heat release rate, and gas species concentrations. Additionally, videos will be recorded with standard and infrared cameras.

Heat Flux Gauges

Six water-cooled Schmidt-Boelter heat flux transducers (Table 2) will be used in the eaves to measure the combined radiative and convective heat flux (Fig. 9). Three gauges will be facing the source structure from the eave boxing in the bay between rafters. Holes will be drilled through the vertical wood panel of the eaves so that the gauge face will be flush with the wood. Three gauges will be facing down from within the underside of the roof overhang with the gauge face flush with the roof slope, not perpendicular to the ground. No heat flux gauges will be in the center eave where the vent will be located.

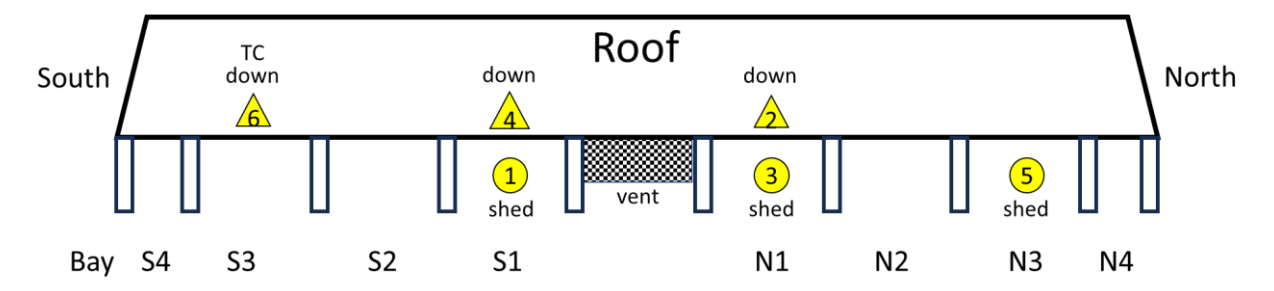


Fig. 9. Location of the 6 heat flux gauges in the eaves. Gauges 1, 3 and 5 face the source structure from the eave bays while gauges 2, 4 and 6 face the source structure from the underside of the roof overhang (figure not to scale).

Thermocouples

Type K, bare bead, 24 AWG thermocouples with a temperature range up to 1250 $^{\circ}$ C with a standard relative uncertainty value of \pm 0.75 $^{\circ}$ C as reported by the manufacturer will be used for these experiments. Three thermocouples will be located horizontally along the back of the eave vent to measure the temperature on the attic side (Table 2). One additional thermocouple on the attic side of the vent will be located higher near the roof above the vent.

One thermocouple will be positioned on the exposed side of the vent. None of the thermocouples located near the eave vent will touch the vent. One thermocouple will be located next to each bi-directional probe (10 probes). There will also be a thermocouple to the

north and south of the target wall at the elevated launch and collection laser instruments to measure reference temperatures.

Bi-Directional Probes

Bi-directional probes will be used to measure the fire induced gas flow velocity along the target wall and through the eave vent (Table 2). Seven bi-directional probes will be located on the wall (Fig. 10); three probes each on the north and south edges of the target wall, and one probe in the middle of the wall. Additionally, three probes will be placed on the attic side of the wall behind the vent, in order to measure the flow through the vent. A thermocouple accompanies each bi-directional probe to determine local air density. Three S-type pitot probes (S-probes) will be placed across the horizontal middle of the target wall near the respective bi-directional probe locations. The EaVE experiments will serve as a case study comparing the performance between bi-directional probes and S-probes during large-scale fire experiments. The nominal uncertainty for the bi-directional and S-probes are 4 % and 2 %, respectively [9].

Table 2. Instrumentation locations related to the target structure where the origin is the bottom center of the

Device	ID	X cm (East +)	Y cm (North +)	Z cm (Up +)	Orientation
Heat Flux Gauge	HF1	0	-30	416	Facing Shed
Heat Flux Gauge	HF2	30	30	416	Facing Down
Heat Flux Gauge	HF3	0	30	416	Facing Shed
Heat Flux Gauge	HF4	30	-30	416	Facing Down
Heat Flux Gauge	HF5	0	90	416	Facing Shed
Heat Flux Gauge	HF6	30	-90	416	Facing Down
Vent Bi-Dir. 1	VBD1	-30	15.2	416	Horizontal (east-west)
Vent Bi-Dir. 2	VBD2	-30	0	416	Horizontal (east-west)
Vent Bi-Dir. 3	VBD3	-30	-15.2	416	Horizontal (east-west)
Wall Bi-Dir. 1	WBD1	0	-213	91	Horizontal (north-south)
Wall Bi-Dir. 2	WBD2	0	213	91	Horizontal (north-south)
Wall Bi-Dir. 3	WBD3	0	-213	208	Horizontal (north-south)
Wall Bi-Dir. 4	WBD4	0	213	208	Horizontal (north-south)
Wall Bi-Dir. 5	WBD5	0	-213	304	Horizontal (north-south)
Wall Bi-Dir. 6	WBD6	0	213	304	Horizontal (north-south)
Wall Bi-Dir. 7	WBD7	0	0	208	Vertical (up-down)
Vent TC 0	ETC	0	0	416	Shed side, front of vent, center
Vent TC 1	ATC	-6	0	416	Attic side, back of vent, center
Vent TC 2	PTC	-11	0	427	Attic side, plywood, center top of plenum
Laser TC N	LTCN	15	305	416	North side with laser
Laser TC S	LTCS	15	-305	416	South side with laser
Vent TC 1	VTC1	-30	15.2	416	Accompany Bi-Dir. Probe
Vent TC 2	VTC2	-30	0	416	Accompany Bi-Dir. Probe
Vent TC 3	VTC3	-30	-15.2	416	Accompany Bi-Dir. Probe
Wall TC 1	WTC1	0	-213	91	Accompany Bi-Dir. Probe
Wall TC 2	WTC2	0	213	91	Accompany Bi-Dir. Probe
Wall TC 3	WTC3	0	-213	208	Accompany Bi-Dir. Probe
Wall TC 4	WTC4	0	213	208	Accompany Bi-Dir. Probe
Wall TC 5	WTC5	0	-213	304	Accompany Bi-Dir. Probe

Device	ID	X cm (East +)	Y cm (North +)	Z cm (Up +)	Orientation
Wall TC 6	WTC6	0	213	304	Accompany Bi-Dir. Probe
Wall TC 7	WTC7	0	0	208	Accompany Bi-Dir. Probe
S-Probe 1	SPB1	0	5	208	Same orientation as WBD7
S-Probe 2	SPB2	0	-213	213	Same orientation as WBD3
S-Probe 3	SPB3	0	213	213	Same orientation as WBD4

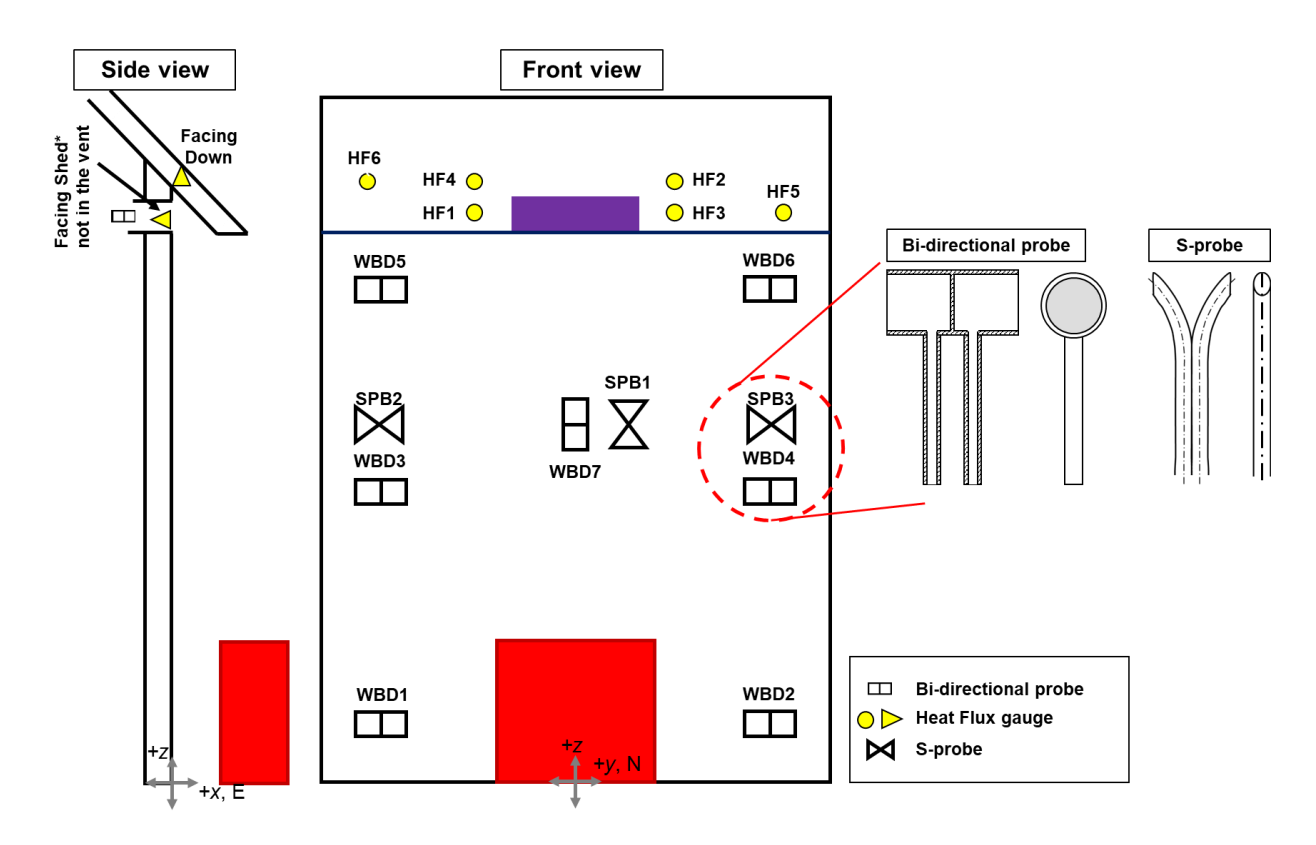


Fig. 10. The heat flux gauge, bi-directional probe, and thermocouple locations on the front face (exposed side) of the target structure (figure not to scale).

Heat Release Rate

The 13.7 m x 15.2 m (45 ft x 50 ft) calorimeter with maximum fire capacity of 20 MW in the NFRL will be used to calculate heat release rate using oxygen consumption calorimetry. The average expanded uncertainty in the normal operating range for the hood for generic combustible fuel is 9.8 %. The uncertainty is valid for near steady-state fires. Transient events (less than 30 s) may have larger uncertainty because of system response time. Detailed information on the NFRL calorimetry measurement system is provided by Bryant and Bundy [10]. Verification (confirmation) of the oxygen consumption calorimetry using fuel consumption calorimetry as a reference will be conducted immediately prior to these experiments using a calibrated gas burner. The heat release data and videos from the experiments will be published in the fire calorimetry database [11].

Video Cameras

Five video cameras will be used to record the experiments (Fig. 11). One video camera will face the experiment directly from the front (camera 1 facing west), one from the front diagonal position (camera 2 facing northwest), and one from the side (camera 3 facing north). One camera will be on an elevated platform behind the target structure (camera 4 facing east). One camera will be mounted on a sled and positioned at the face of the wall facing upwards towards the eave vent (camera 5). It will be pulled on the sled, away from this position, if it becomes exposed to direct flame.

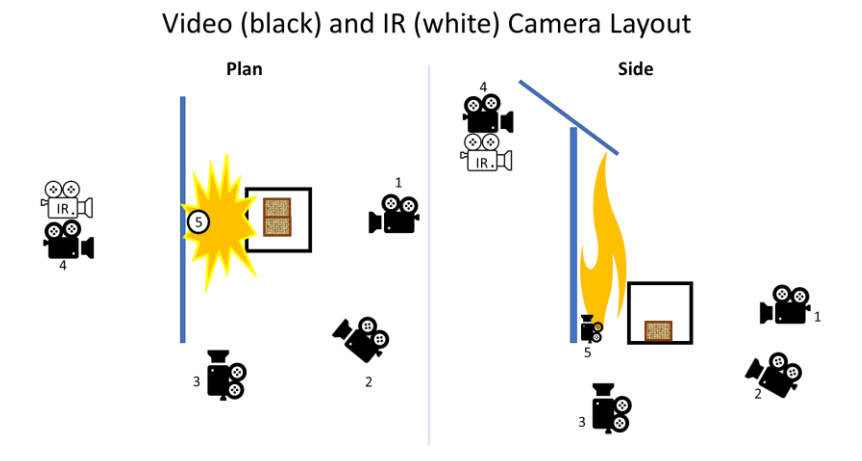


Fig. 11. The positions of the 5 video cameras (black) including the video camera position at the face of the target structure, and one IR camera (white) (figure not to scale).

Infrared Camera

A high-speed mid-wavelength infrared camera (FLIR SC8300HD) will be mounted on the elevated platform behind the target structure (facing east) to record thermal images for qualitative monitoring (Fig. 11). It will be aimed at the back of the eave vent to capture the thermal image at the vent. The field of view of the IR camera will be limited by the position of the elevated platform at a safe distance behind the target structure.

Data Acquisition System (DAQ)

A National Instruments (NI) cDAQ-9184 data acquisition (DAQ) chassis with NI-9213 I/O-Modules for thermocouples and NI-9215 modules for sensors with voltage outputs will be used to sample the output from heat flux gauges and thermocouples at a frequency of 1 Hz. The heat release rate (HRR) measurements from the calorimeter will be made on an independent data collection system called the Modular In-Situ Data Acquisition System (MIDAS). Uncertainties related to the DAQ are expected to be orders of magnitude lower than those from the other measurements [2].

California Building Code Chapter 7A Section 706A specifies that the maximum temperature of the unexposed side of a WUI eave vent shall not exceed 350 °C [6]. Therefore, a red-light

indictor will be illuminated in the DAQ system to visually represent when the maximum temperature is achieved behind the vent and for the experiment to be terminated.

Open-Path Laser Spectroscopy

An open-path laser spectrometer will be deployed to make gas-phase concentration (CO_2 and H_2O) and temperature measurements in both the eave and the attic space of the target wall structure. The spectrometer is custom-built and equipped with near-infrared laser diodes for molecular absorption measurements and a visible alignment laser. The instrument design will closely follow previous field demonstrations [12].

To incorporate the laser instruments into the experiments, platforms will elevate the instruments to the required height (for additional details see Appendix C). One platform will be placed on either side of the target structure (north and south) to accommodate optics used to send and receive laser light. In this configuration (Fig. 12), the laser will perform a single pass of the target structure (i.e., optics to send laser light are on one platform (north) and the optics to receive laser light are on the other (south)). The distance between the sending/receiving instruments will be approximately 10 m (33 ft). The elevated optical components will be protected from splashing water during fire suppression if required at the end of the experiments.

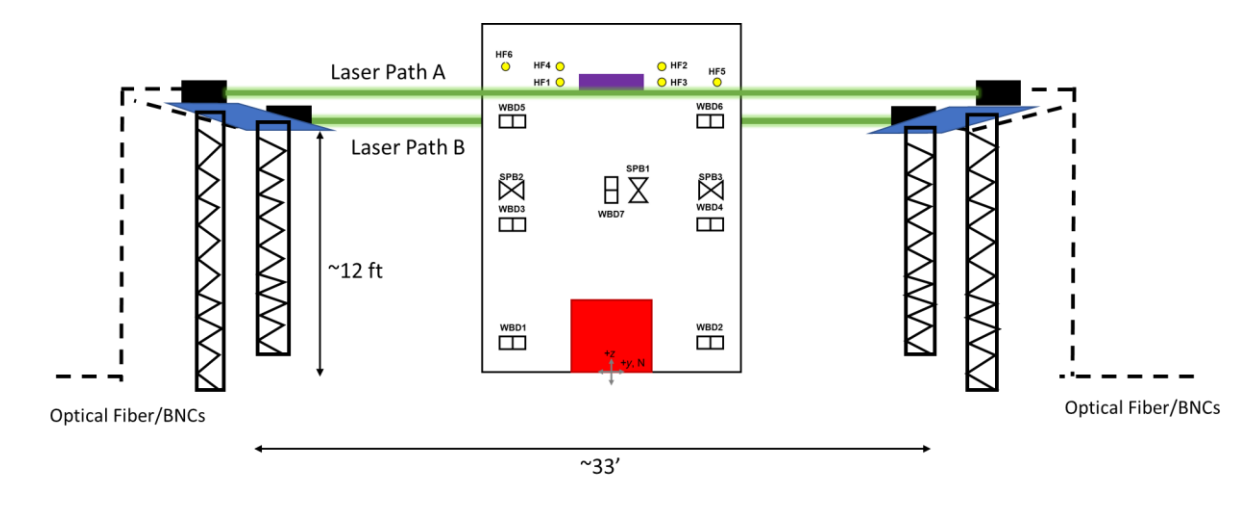


Fig. 12. Unscaled mockup of laser instrument incorporated into the target structure set up. The target structure is shown in the center with laser launch and collection platforms on either side. The laser stands are anchored to the floor supporting the elevated platforms approximately 3.7 m (12 ft) above ground level (figure not to scale).

At the target structure, the distance between the laser beam passing under exterior eave bays (path A) and behind the eave vent, on the attic side (path B), will be approximately 0.81 m (32 in) (Fig. 13). The laser path B will be elevated an additional 20 cm (8 in) compared to path A, so as to pass through the concentrated gases exiting the plenum behind the vent (Fig. 14).

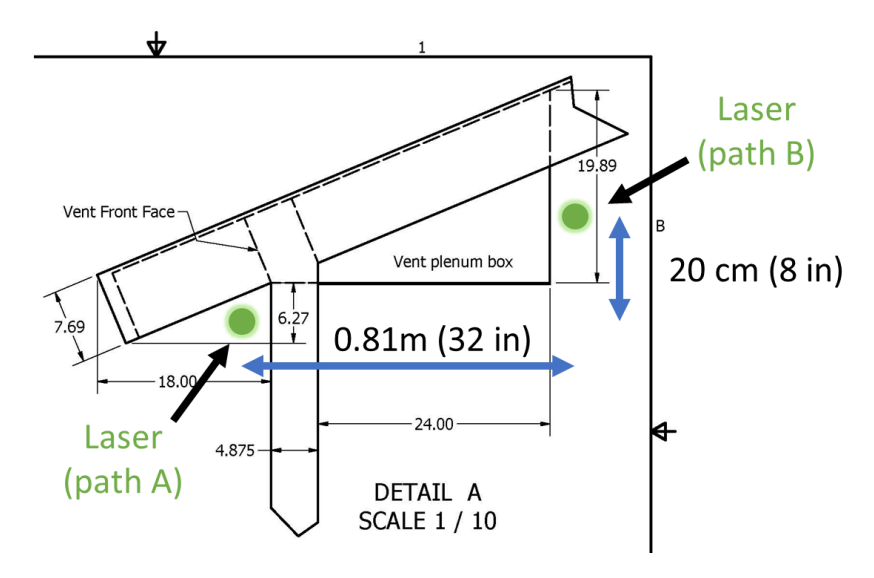


Fig. 13. Horizontal and vertical distances between laser path A through the eaves and path B behind the eave vent.

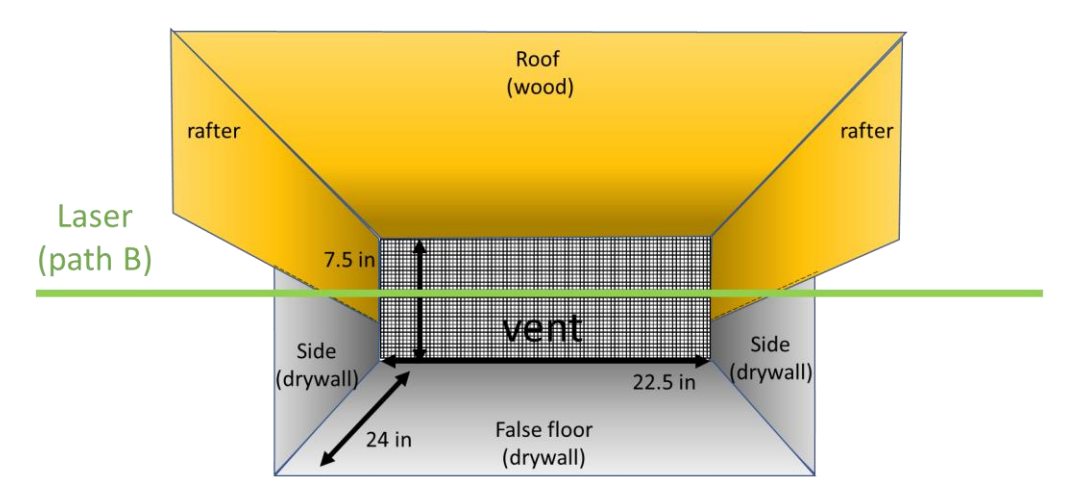


Fig. 14. Laser path B behind the eave vent passes just under the rafters to pass through concentrated gases (figure not to scale; 1 in = 2.54 cm).

3.2 Technical Issues

The following items have been identified as technical issues that will need to be addressed prior to the experiments.

- Open-path absorption spectroscopy will attempt to quantify CO₂, water, and gas-phase temperature on the exterior side of the eave vent as well as on the interior (attic) side.
- Positioning of the Narrow metal shed so that the heat and flame will be centered under the eave vent. Based on the geometry of the Narrow shed, it will need to be offset from the wall center (to the north).

- A thermocouple will be installed on the interior side of the eave vent to measure the temperature on the attic side of the vent. When the thermocouple measures 350 °C, then the vent has failed (according to Chapter 7A [6]) and the test will end.
- The fuel loading will be varied to expose the eave vent to a range of radiant and convective heat. If additional increments of fire exposure are required, then the shed doors may need to be adjusted to a partially closed configuration.

3.3 Source-Structure-Only Experiment Configuration

A set of 6 preliminary experiments will be conducted with associated measurements without the target structure (Appendix D). Three different galvanized steel sheds will be used with a pre-determined number of 1-A wood cribs as the fuel load under the 20 MW calorimetry hood.

3.3.1 Objective

The objectives of the preliminary experiments are to:

- 1. Determine the effect of fire and heat on the open-path absorption spectrometer.
- 2. Determine the position of the Narrow shed so that the heat and smoke plume will be directed under the eave vent.
- 3. Evaluate the sensitivity of the 20 MW calorimetry measurements.
- 4. Evaluate reproducibility of the shed burn experiments.

3.3.2 Instrumentation

Since the target structure will not be included in the preliminary experiments, a limited number of measurements will be made. The instrumentation used for preliminary experiments will include:

- Fire calorimetry under the 20 MW hood to measure heat release rate.
- Six heat flux gauges arranged in front of the shed door (Fig. 15).
- Video cameras and an infrared camera to record the experiments.
- The DAQ to collect available data.
- The open-path absorption spectrometer to measure concentrations of CO₂ or H₂O and temperature in the same elevated location as if the target structure is in place (Fig. 15).

3.3.3 Preliminary Experiment Matrix

Six shed burn experiments will be conducted with various fuel loadings. For all preliminary experiments the shed doors will be kept fully open. See Section 3.1.3 for fuel loading configurations. The heat release rate will be measured, and six heat flux gauges will be used (Fig. 15) at nominal heights of 1 m (gauges 1, 3 and 5) and 3 m (gauges 2, 4 and 6).

- 1. **Experiment 1**: A Narrow shed with a medium fuel load of 4 cribs. The shed door will be facing the heat flux gauges, instead of the experiment configuration where the shed door will face 90° to the target structure. The effect of increased fuel load on the flame and smoke plume direction will be observed.
- 2. **Experiment 2**: A Very Small shed with a high fuel load of 6 cribs. This experiment matches the previous 1B-SVSh0 experiment with 6 cribs [2]. The purpose of this experiment is to compare the NISSE and current experiment results.
- 3. **Experiment 3**: A Narrow shed with a low fuel load of 2 cribs. The shed door will be facing the heat flux gauges, instead of the experiment configuration where the shed door will face 90° to the target structure. The flame and smoke plume direction will be observed for shed placement under the eave vent.
- 4. **Experiment 4**: A Closet shed with a low fuel load of 2 cribs placed side by side. The purpose of this experiment is to evaluate reproducibility of the 1B-SCIO experiment with 2 wood cribs conducted during the NISSE series [2].
- 5. **Experiment 5**: A Narrow shed with a high fuel load of 6 cribs. The shed door will be facing the heat flux gauges, instead of the experiment configuration where the shed door will face 90° to the target structure. The effect of high fuel load on the flame and smoke plume direction will be observed.
- 6. **Experiment 6**: A Very Small shed with a low fuel load of 4 wood cribs. This set of experiment parameters was not tested previously. Previously, metal Very Small sheds were loaded with 6 cribs for fuel ([2] test #6, 1B-SVSh0).

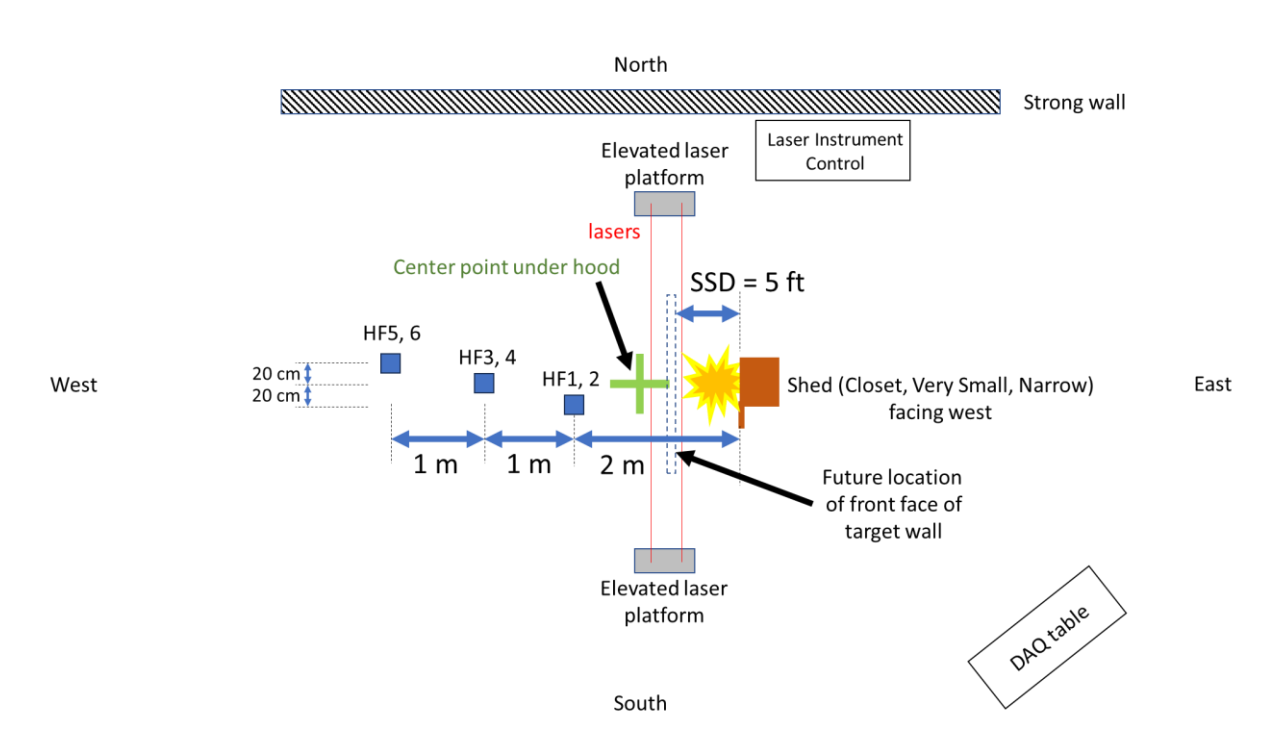


Fig. 15. Plan view of the preliminary experiment layout with the sheds facing the heat flux gauges (figure not to scale).

3.4 Eave Vent Experiment Matrix

3.4.1 Objective

The objective of these experiments is to characterize the performance of a fire-resistant eave vent with an intumescent coating exposed to fire from the source structure. The experiment objectives will be accomplished by performing the following series of experiments using only noncombustible steel sheds of varying sizes and varying fuel loads (wood cribs). It is anticipated that there may be up to 16 experiments in this series (Appendix D).

3.4.2 Experiment Parameters

The primary experiment parameters are summarized in Table 3. In general, high fuel loadings will be burned before low fuel loadings; if a high fuel load does not cause a vent failure, then the low fuel load experiments are unnecessary. See Section 3.1.3 for fuel loading configurations. All sheds will have a 0 degree orientation (door facing the target structure), except the Narrow shed will be oriented with the shed door 90 degrees to the target structure. The shed doors will be in the fully open configuration, unless it is determined that a reduced fire exposure is required, and a shed door may be positioned in a partially open configuration. The Closet and Very Small sheds will be positioned with a SSD of 1.5 m (5 ft), while the Narrow shed will be positioned against the target structure with a SSD of 0 m.

Source Structure Material	Source Structure Size (D x W x H) ft, ft ³	Fuel Loading	
	Closet (3 x 6 x 4), 66	Low	
Galvanized Steel	Very Small (5 x 6 x 6), 146	Medium	
	Narrow (6.5 x 4 x 5), 161	High	

Table 3. Primary experiment parameters (1 ft = 0.0305 m).

The experiment naming convention used previously [2, 4] will follow the convention as follows: *Phase* (EAVES_A) - *Material* (Steel (S)), *Size* (Closet (C), Very Small (VS), Narrow (N)), *Fuel Load* (low (I), medium (m), high (h)), *Wind Speed* (# mi/h) - *SSD* (# ft) - *Replicate* (R#). The letter "R" followed by a number at the end of the experiment name indicates a test replicate. If the eave vent fails, the experiment conditions will be replicated twice more (3 total failures), assuming there is time and materials. For example, the first repeat for a Narrow metal shed with high fuel loading and a 0 SSD will have an experiment number EAVES_A-SNh0-0-R1.

3.4.3 Experiment Decision Matrix

The following conditional statements and flowchart (Fig. 16) were developed to facilitate the decision making for the selection of experiments based on results. The sequencing of experiments as prioritized using Fig. 16 is shown in Table 4.

IF C with high fuel loading (FL) fails (1st time), THEN repeat C with high FL (2nd time)

IF C with high FL fails (3rd time), THEN C with low FL (1st time)

IF C with low FL does not fail, THEN VS with low FL

IF C with high FL does not fail (1st time), THEN VS with high FL (1st time)

IF VS with high FL fails (1st time), THEN repeat VS with high FL (2nd and 3rd time)

IF VS repeatably fails, THEN VS with low FL (1st time)

IF VS with low FL does not fail, THEN N with high FL (1st time)

If VS with high FL does not fail, THEN N with high FL (1st time)

If N with high FL fails (1st time), THEN repeat N with high FL (2nd and 3rd time)

If N repeatably fails with high FL, THEN N with medium FL (1st time)

If N with medium FL fails (1st time), THEN repeat N with medium FL (2nd and 3rd time)

If N repeatably fails with medium FL, THEN N with low FL (1st time)

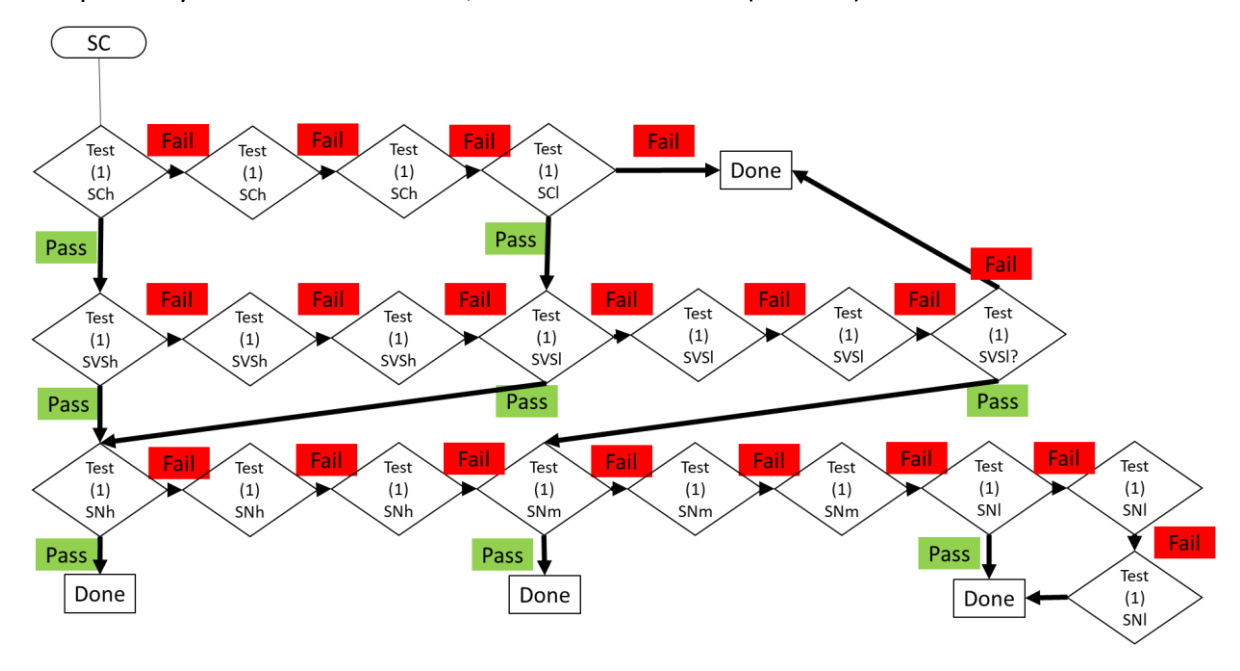


Fig. 16. Conditional flowchart for experiment matrix. Vent failures will be repeated a total of three times.

Table 4. Experiment sequence based on flowchart.

Serial	Experiment	Source	Source	Fuel Loading	SSD
Number	ID	Structure Material	Structure Size	(# of cribs)	(ft)
1	SCh0-5		Closet	High (4)	5
2	SCI0-5		Closet	Low (2)	5
3	SVSh0-5		Very Small	High (6)	5
4	SVSI0-5	Steel	Very Small	Low (4)	5
5	SNh0-0		Narrow	High (6)	0
6	SNm0-0		Narrow	Med (4)	0
7	SNIO-0		Narrow	Low (2)	0

3.5 Modeling

Previous modeling results contributed towards these planned experiments:

- 1. Provided input data to guide the laser instrumentation setup and helped define laser parameters.
- 2. Helped determine target structure parameters such as the target wall width.
- 3. Assessed the influence of open outlets on the rear side of attics and examined how varying the size of these openings affected the fire dynamics.
- 4. Analyzed whether the presence or absence of an attic affected wind flow and consequential heat exposure, and investigated how the size of the attic may impact overall conditions.

The results from these experiments will be used to verify and improve numerical models that were developed during the previous indoor [2] and outdoor experiments [4]. The measurement results from this study will be used as input for model verification (Appendix E).

4. Uncertainty of Measurements

The measurements of heat release rate, heat fluxes, temperatures, times, gas and airflow velocities, and distances have associated uncertainties. Measurement uncertainties have several components that are typically grouped into two categories based on the method used to estimate their value. Type A uncertainties are evaluated by statistical methods, and Type B uncertainties are evaluated by other means, often based on scientific judgement using all available relevant information [13]. The component standard uncertainty includes resolution, calibration, installation, and random errors. The resolution is the minimum change in the data measurement the instrument can exhibit. Calibration error includes uncertainties from sensor calibration. The resolution and calibration uncertainties were derived from instrument specifications (Type B). Uncertainty due to the installation method was estimated based on engineering judgment (Type B) considering misalignment, quality of the sensor mounting method, and previous data.

Given the nature of experiments and hence the singular measurements in this study, the evaluation of Type A uncertainties was not feasible for the majority of measurements. Most uncertainties reported herein are Type B uncertainties, either estimated through scientific judgment or obtained from the literature.

Type K thermocouples used in these experiments have an inherent standard uncertainty for the temperature measurements reported by the manufacturer as \pm 0.75 %. Additional uncertainties in measured temperature are primarily due to radiative heating and cooling of the thermocouple bead that causes it to respond to phenomena other than the surrounding gas temperature. Due to the nature of fire testing, the thermal environment surrounding a given thermocouple is difficult to characterize. These uncertainties will overwhelm the inherent uncertainties in the thermocouple described earlier.

The FLIR camera has a standard uncertainty of 2 °C (4 °F) or 2 % of the measured temperature. The uncertainties in temperature measurement using the IR camera may result from the emissivity value employed, reflected temperature, distance between the camera lens and the target surface, ambient temperature, transmittance, and calibration accuracy. The FLIR temperature measurements will be used qualitatively, and these additional factors will not be quantified.

The average expanded uncertainty in measuring the heat release rate in the normal operating range of the 20 MW (13.7 m x 15.2 m) hood for generic combustible fuels is 9.8 %. This uncertainty is valid for near steady state fires. Transient events (less than 30 s) may have more significant uncertainty because of system response time. Bryant and Bundy [10] provide detailed information on the NFRL calorimetry measurement system.

The nominal uncertainty for the bi-directional and S-probes are 4 % and 2 %, respectively [9].

The relative expanded uncertainty reported by the manufacturer for the heat flux gauges is \pm 3 % of the gauge sensitivity (the slope of the calibration curve) with a coverage factor of 2. This would result in an uncertainty of about 4 kW/m² for a nominal reading of 140 kW/m². The main sources of uncertainty for the total heat flux measurements are: (1) the uncertainty of the

NIST TN 2288 May 2024

analog/digital conversion, (2) uncertainty in the calibration, and (3) uncertainty due to soot deposition on the sensing surface of the gauge [14].

The uncertainty in the A/D conversion is inherent to the data acquisition system. It is system-specific and is associated with the digitization of the analog signals from the gauge. This type of uncertainty is negligible. The uncertainty due to soot deposition is more challenging to quantify. The amount of soot deposition depends on many parameters, such as the location of the gauge, the flow field and temperature fields near the gauge, the duration of an experiment, and the soot volume fraction. No attempt will be made to quantify the soot effect on heat flux measurements for these experiments. Additional uncertainty due to flame impingement on the gauges is considered negligible.

The structure separation distances (SSDs) between the target wall and the source structure and the distance between the source structure and instrumentation including the heat flux gauge will be measured using a tape measure. Sources of uncertainty include the placement of the tape measure and the ability to adjust the positions of the source structure and sensors accurately. The construction dimensions are rounded to the nearest tenth. The expanded uncertainty for engineering measurements with a confidence level of 95 % was estimated as $\frac{1}{2}$ inch (1.2 cm). For longer tape measures, the expanded uncertainty was \pm 1 in (\pm 2.54 cm).

The users of this report are advised to be informed that the experimental results presented in this report are either raw data or the statistics of raw data acquired by the measurement systems. Incorporating the measurement uncertainty reported herein into the validation of predictive models is highly recommended.

5. Data Management

The data generated from these experiments will be useful for WUI code development and for future modeling purposes to better understand fire spread in WUI communities. To facilitate data availability for interested parties, an online repository will be created to store the project description, detailed experiment plan, experiment data, instrumentation, calibration and verification reports, safety documents, images, and video clips. A preliminary data management and quality assurance plan is provided elsewhere [1].

6. References

- [1] Maranghides A, Nazare S, Link E, Prasad K, Hoehler M, Bundy M, Hawks S, Bigelow F, Mell W, Bova A, McNamara D, Milac T, Gorham D, Hedayati F, Raymer B, Frievalt F, Walton W (2021) Structure Separation Experiments Phase 1 Preliminary Test Plan. NIST Technical Note 2161. National Institute of Standards and Technology, Gaithersburg, MD. https://doi.org/10.6028/NIST.TN.2161
- [2] Maranghides A, Nazare S, Link E, Hoehler M, Bundy M, Hedayati F, Gorham D, Monroy X, Morrison M, Mell W, Bova A, Milac T, McNamara D, Hawks S, Bigelow F, Raymer B, Frievalt F, Walton W (2022) Structure Separation Experiments: Shed Burns without Wind. NIST Technical Note 2235. National Institute of Standards and Technology, Gaithersburg, MD. https://doi.org/10.6028/NIST.TN.2235
- [3] Maranghides A, Nazare S, Link E, Bundy M, Chernovsky A, Johnsson E, Butler K, Hawks S, Bigelow F, Mell W, Bova A, McNamara D, Milac T, Gorham D, Hedayati F, Raymer B, Frievalt F, Walton W (2022) NIST Outdoor Structure Separation Experiments (NOSSE): Preliminary Test Plan. NIST Technical Note 2199. National Institute of Standards and Technology, Gaithersburg, MD. https://doi.org/10.6028/NIST.TN.2199
- [4] Maranghides A, Nazare S, Butler KM, Johnsson EL, Link E, Bundy M, Chernovsky A, Walton WD, Hawks S, Bigelow F, Mell W, Bova A, McNamara D, Milac T, Raymer R, Frievalt F (2023) NIST Outdoor Structure Separation Experiments (NOSSE) with Wind. NIST Technical Note 2253. National Institute of Standards and Technology, Gaithersburg, MD. https://doi.org/10.6028/NIST.TN.2253
- [5] ASTM E 2886- Standard Test Method for Evaluating the Ability of Exterior Vents to Resist the Entry of Embers and Direct Flame Impingement.
- [6] California Building Code-Chapter 7A-Materials and construction methods for exterior wildfire exposure. Available at https://codes.iccsafe.org/content/CABC2022P3/chapter-7a-sfm-materials-and-construction-methods-for-exterior-wildfire-exposure#CABC2022P3 Ch07A Sec706A
- [7] UL 711, 8th Edition, January 5, 2023 UL Standard for Safety Rating and Fire Testing of Fire Extinguishers.
- [8] Walton W. (1988) Suppression of Wood Crib Fires with Sprinkler Sprays: Test Results. NBSIR 88-3696, National Bureau of Standards, U.S. Department of Commerce.
- [9] Di Cristina Torres G, Bryant RA (2024) Comparison of flow measurement devices for large fire experiments. NIST Technical Note 2285. National Institute of Standards and Technology, Gaithersburg, MD. https://doi.org/10.6028/NIST.TN.2285
- [10] Bryant RA and Bundy MF (2019) The NIST 20 MW Calorimetry Measurement System for Large-Fire Research. NIST Technical Note 2077. National Institute of Standards and Technology, Gaithersburg, MD. https://doi.org/10.6028/NIST.TN.2077
- [11] NIST Fire Calorimetry Database (FCD) https://doi.org/10.18434/mds2-2314
- [12] Bailey DM, Adkins EM and Miller JH (2017). An open-path tunable diode laser absorption spectrometer for detection of carbon dioxide at the Bonanza Creek Long-Term Ecological Research Site near Fairbanks, Alaska. Appl. Phys. B 123, 245. https://doi.org/10.1007/s00340-017-6814-8.

- [13] Taylor BN, Kuyatt CE (1994) Guidelines for evaluating and expressing the uncertainty of NIST measurement results. NIST Technical Note 1297. National Institute of Standards and Technology, Gaithersburg, MD. https://dx.doi.org/10.6028/NIST.TN.1297
- [14] Maranghides A and Johnsson EL (2008) Residential Structure Separation Fire Experiments. NIST Technical Note 1600. National Institute of Standards and Technology, Gaithersburg, MD. https://doi.org/10.6028/NIST.TN.1600

Appendix A – Target Structure Design and Specifications

Structural Stability of EaVE Test Target Wall

This calculation is done to check the structural stability of the support frame under the load transferred from the EaVE test target wall and roof. Fig. 17 shows the target wall and the support frame. The wall as well as the roof are 16-ft long.

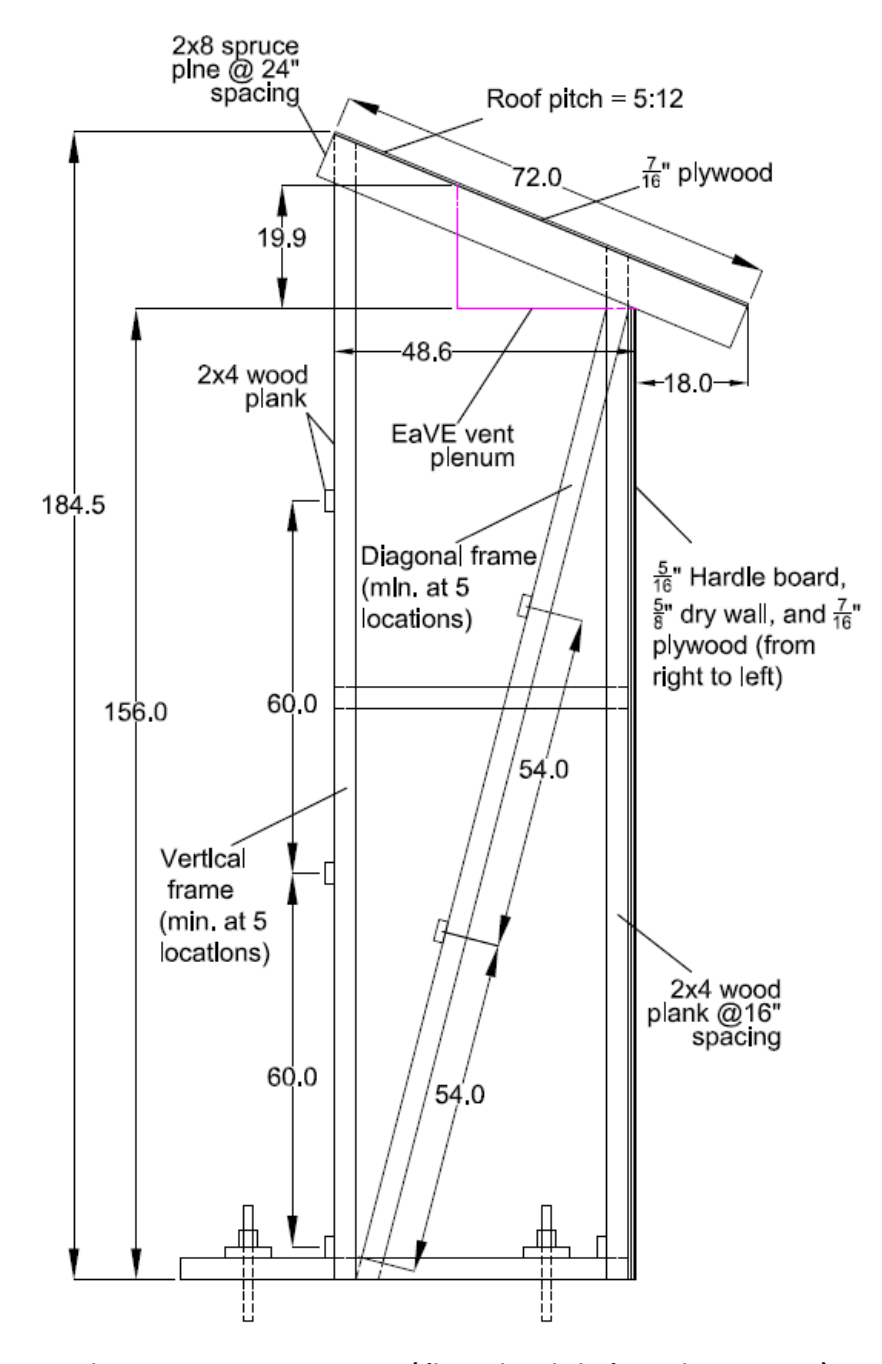


Fig. 17. EaVE Target Structure (dimensions in inches; 1 in. = 2.54 cm)

1] Weight of Materials

Density of Hardie board (5/16 in. thick) =83 lb/ft³ (from Jameshardie.com)

Density of drywall (5/8 in. thick) =42 lb/ft 3

Density of plywood (7/16 in. thick OSB) =40 lb/ft³

Density of spruce pine (2×8) =33 lb/ft³

Density of Douglas-fir wood plank (2×4) =30 lb/ft³

Surface area of the target wall = $13 \text{ ft} \times 16 \text{ ft}$

(Area of Hardie board, drywall, or plywood) =208 ft²

Total weight of the wall = $208 \text{ ft}^2 \times [83 \text{ lb/ft}^3 \times 5/16 \text{ in.} + 42 \text{ lb/ft}^3$

 $\times 5/8 \text{ in } + 40 \text{ lb/ft}^3 \times 7/16 \text{ in}$

=450 lb + 455 lb + 303 lb

=1208 lb

Number of 2×4 wood planks (attached to wall) = 13

Weight of 2×4 wood planks = 13×30 lb/ft³ × [1.5 in. ×3.5 in. ×13 ft]

=185 lb

Weight of (wall + wood planks) = 1208 lb + 185 lb

=1393 lb

Weight of plywood of the roof = $40 \text{ lb/ft}^3 \times [6 \text{ ft} \times 16 \text{ ft} \times 7/16 \text{ in.}]$

=140 lb

Number of 2×8 spruce pine wood planks = 10

Weight of 2×8 spruce pine wood planks = 10×33 lb/ft³ × [1.5 in. ×7.5 in. ×6 ft]

=155 lb

Total weight of roof = 140 lb + 155 lb

=295 lb

2] Stability of 2×4 wood planks attached to the wall panel

Modulus of Rupture (MOR) of 2×4 Douglas-fir wood plank (with a maximum moisture content of 12%, from Table 5-3b of USDA handbook, 2010)

Modulus of Rupture, MOR = 12400 psi

Number of 2×4 wood planks (1.5 in. \times 3.5 in.) = 13

The effective length for bending members from Table 3.3.3 of AWC-NDS (2018)

Effective length = 1.84 (13 ft)

= 287 in.

 $MOR = 12400 \ psi = \frac{\frac{1}{8} * \left(\frac{W_{max}}{16 \ ft} * (287 \ in)^{2}\right) \left(\frac{3.5 \ in}{2}\right)}{13 * \frac{1}{12} * 1.5 \ in * (3.5 \ in)^{3}}$

Maximum weight of wall panel, W_{max} = 9206 lb

Factor of Safety (FOS) for bending = 9206 lb/1393 lb

=6.6 (Ok!)

Compression edge of the vertical wood planks are attached to the plywood over their entire length of wood planks. Hence, no need to have cross planks for the vertical 2×4 wood planks attached to the wood panel.

3] Stability of vertical support wood frame for axial load from roof

Total weight of roof = 295 lb

Axial load from roof to the vertical wood frame = 295 lb / 2

= 148 lb

Angle of roof with horizontal = $tan^{-1}(5/12)$

=22.62°

Height of wooden frame = $13 \text{ ft} + 6 \text{ ft} \times \sin (22.62^\circ)$

=15.3 ft

=183.7 in.

From Table 5-3b of USDA handbook-2010,

Elastic modulus of 2×4 Douglas-fir wood plank, E_L = 1950 ksi

From Table 4.3.1 of AWC-NDS (2018),

Resistance factor for elastic modulus, ϕ = 0.85

Minimum elastic modulus, E_{min} = 0.85×1950 ksi

= 1658 ksi

From Table G1 of AWC-NDS (2018),

The column stability factor 'Ke' = 2.4

Limiting un-braced length for 2×4 in $= l_{e.max.w} = 50 \times 1.5$ in

the weak-axis direction = 75 in

Limiting un-braced length for 2×4 in $= l_{e.max.s} = 50 \times 3.5$ in

the strong- axis direction = 175 ir

Provide lateral bracing (as shown in Fig.1) every 5 ft height in the 1.5 thickness direction to satisfy $l_{e.max.w}$ = 75 in.

Calculating column stability factor using equation (3.7-1) of AWC-NDS (2018) handbook From Table 5-3b of USDA handbook-2010,

Compressive strength Fc^* of 2 × 4 wood plank = (0.9) (7230 psi)

$$F_{CE} = \frac{0.822 * E_{min}}{\left(\frac{K_e * l}{d}\right)^2}$$

$$F_{CE} = \frac{0.822 * 1658 \, ksi}{\left(\frac{2.4 * 183.7 \, in.}{3.5 \, in}\right)^2}$$

= 85.9 psi

 F_{CE}/F_{C}^{*} = 85.9 ksi / 6507 psi

=0.0132

C = 0.8 (for sawn lumber)

From Equation (3.7-1) of AWC-NDS (2018),

$$C_{P} = \frac{1 + F_{CE}/F_{C}^{*}}{2 * C} - \sqrt{\left(\frac{1 + F_{CE}/F_{C}^{*}}{2 * C}\right)^{2} - \left(\frac{F_{CE}/F_{C}^{*}}{C}\right)^{2}}$$

$$C_P = \frac{1 + 0.0132}{2 * 0.8} - \sqrt{\left(\frac{1 + 0.0132}{2 * 0.8}\right)^2 - \left(\frac{0.0132}{0.8}\right)}$$

 $C_P = 0.01316$

Axial load capacity of a 2×4 wood plank (183.7 in),

$$C_{\text{vertical}} = (0.01326) (6507 \text{ psi}) (1.5 \text{ in} \times 3.5 \text{ in})$$

NIST TN 2288 May 2024

For 5 wood planks $C_{\text{vertical frame}} = 5 \times 451 \text{ lb} = 2255 \text{ lb}$

Factor of safety = 2255 lb / [(295 lb) / 2]

= 15.3 Ok!

4] Stability of diagonal wood frame

Vertical load that needs to be carried by the

diagonal wood frame $= \frac{1}{2}$ of weight of wood panel

+ 1/2 of weight of roof

= ½ × 1393 lb + ½ × 295 lb

= 844 lb

Angle of diagonal frame with horizontal = tan^{-1} [5 ft × cos (22.62°) /13 ft]

= 19.54°

Arial load on the diagonal frame = 844 lb/ cos (19.54°)

= 895 lb

Length of diagonal frame = $13 \text{ ft /cos } (19.54^{\circ})$

= 13.79 ft

= 165.5 in

Calculating column stability factor using equation (3.7-1) of AWC-NDS (2018) handbook,

Compressive strength F_c^* of 2 × 4 wood plank = (0.9) (7230 psi)

= 6507 psi

$$F_{CE} = \frac{0.822 * E_{min}}{\left(\frac{K_e * l}{d}\right)^2}$$

$$F_{CE} = \frac{0.822 * 1658 \, ksi}{\left(\frac{2.4 * 165.5 \, in.}{3.5 \, in}\right)^2}$$

= 105.8 psi

 F_{CE}/F_{C}^{*} = 105.8 ksi / 6507 psi

=0.01626

C = 0.8 (for sawn lumber)

From Equation (3.7-1) of AWC-NDS (2018),

$$C_{P} = \frac{1 + F_{CE}/F_{C}^{*}}{2 * C} - \sqrt{\left(\frac{1 + F_{CE}/F_{C}^{*}}{2 * C}\right)^{2} - \left(\frac{F_{CE}/F_{C}^{*}}{C}\right)}$$

$$C_P = \frac{1 + 0.01626}{2 * 0.8} - \sqrt{\left(\frac{1 + 0.01626}{2 * 0.8}\right)^2 - \left(\frac{0.01626}{0.8}\right)}$$

 $C_P = 0.0162$

Arial load capacity of a 2×4 diagonal wood plank (165.5 in),

 $C_{diagonal}$ = (0.0162) (6507 psi) (1.5 in × 3.5 in)

= 553 lb

For 5 diagonal wood planks, $C_{diagonal frame} = 5 \times 553 \text{ lb} = 2765 \text{ lb}$

Factor of safety = 2765 lb / 895 lb

= 3.1 Ok!

Summary:

1. Total weight of wall panel = 1393 lb

2. Total weight of roof = 295 lb

- 3. Factor of safety for wood planks attached to wall panel to resist bending = 6.6
- 4. Factor of safety of vertical wood frame to resist half of the load from roof =15.3
- 5. Factor of safety of diagonal wood frame to resist load from roof and wall panel.

=3.1

6. Need to attach 2×4 wood planks to the vertical wood frame and diagonal wood frame across the 1.5 in thickness to have a maximum un-braced length of 75 in (as shown in Fig. 17)

Wall – Assembly

The target wall will be constructed as was done previously [1,2] with the following materials (from the interior to the exterior) (Fig. 18):

- 5/8" drywall, one layer
- 2 in x 4 in wood studs
- 3.5 in, R-14, 16 in wide, fiberglass insulation
- 7/16" OSB sheathing, one layer
- 5/8" noncombustible sheathing board, one layer
- 5/16" Fiber cement panel siding (hardie board)

These materials were selected from those listed on the California Building Materials listing website (https://osfm.fire.ca.gov/what-we-do/fire-engineering-and-investigations/building-materials-listing).

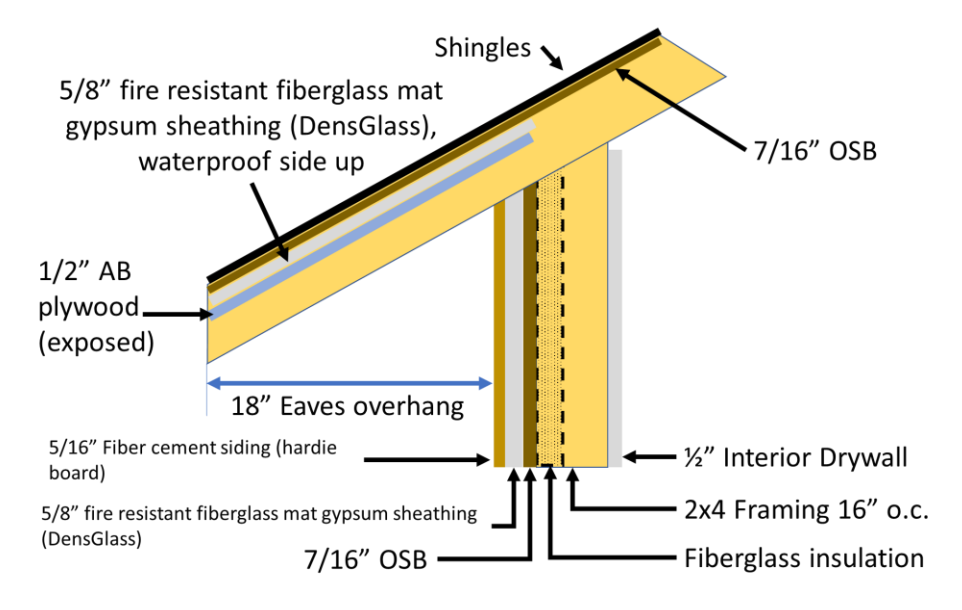


Fig. 18. Target wall construction details with roof overhang (figure not to scale).

Roof

The roof will be built in compliance with California Chapter 7A [6] requirements and will be the same construction as done for the previous experiments [1-4]. Class A asphalt single will be used on 61 cm (24 in) on center rafters.

https://www.gaf.com/en-us/roofing-materials/residential-roofing-materials/shingles/royal-sovereign

Roof underlayment with Class A fire rating (UL 790) will be used.

https://www.gaf.com/en-us/roofing-materials/residential-roofing-materials/roof-deck-protection/tiger-paw-premium-roof-deck-protection

Commercially available K-style black aluminum gutters (nominal 15 cm (6 in) by 2.4 m (8 ft) nominal sections) will be used with aluminum gutter hangers and screws.

https://www.homedepot.com/p/Spectra-Metals-6-in-x-8-ft-K-Style-Black-Aluminum-Gutter-6KBK8/206305103

Black aluminum drip edge flashing 0.48 mm (0.019 in) nominal thickness will be used.

https://www.homedepot.com/p/Amerimax-Home-Products-F5M-x-10-ft-Black-Aluminum-Drip-Edge-Flashing-5564535120/203484742

Eaves

An open eave construction with an eave overhang distance of approximately 46 cm (18 in) will be used. The eave height of 4.3 m (13 ft) above ground level (AGL) assumes 3 m (9 ft) ceilings and a crawlspace as shown in Fig C-3 of the NISSE test plan [1] and Fig. 123 of the NISSE report [2] (Fig. 19).



Fig. 19. Eave height for a single-story family residence [2].

NIST TN 2288 May 2024

Eave Vent

Only a Chapter 7A WUI compliant eave vent with an intumescent coating will be used. These fire stopping eave vents have nominal dimensions of 7.5 in by 22 in and are generally recommended for residential construction in WUI areas.

Gray Fire Block Specialty Sealant (3M part number FB136) will be applied around the eave vent from the exterior side of the target wall.

https://www.3m.com/3M/en_US/p/d/v000292995/

Appendix B – Source Structures

Closet Sheds

Arrow, Storboss 6 ft. x 3 ft. Charcoal Galvanized Steel Horizontal Shed

https://www.homedepot.com/p/Arrow-Storboss-6-ft-x-3-ft-Charcoal-Galvanized-Steel-Horizontal-Shed-STB63CC/314130632

Very Small Sheds

Arrow, 6 ft. H x 5 ft. D x 5.5 ft. W EZEE Galvanized Steel Low Gable Shed in Charcoal/Cream Trim with Snap-IT Quick Assembly

https://www.homedepot.com/p/Arrow-6-ft-H-x-5-ft-D-x-5-5-ft-W-EZEE-Galvanized-Steel-Low-Gable-Shed-in-Charcoal-Cream-Trim-with-Snap-IT-Quick-Assembly-EZ6565LVCCCR/303011036

Narrow Lean-to Sheds

Arrow, Yardsaver 4 ft. W x 7 ft. D White Galvanized Metal (steel) Storage Shed

https://www.homedepot.com/p/Arrow-Yard-Saver-4-ft-W-x-7-ft-D-White-Galvanized-Metal-Storage-Shed-YS47-A/100072804

Appendix C - Elevated Platform Design

Structural stability of the laser platform

This calculation is done to check the flexural capacity of the $L5\times5\times3/4$ in. angle to carry the load from the two lasers mounted 32-in. apart on the laser platform as shown in Fig. 20. The angle has 1-1/16 in. diameter holes, spaced at 3 in. over the entire length of the angle. The center of the 1-1/16 in. diameter holes in the vertical leg of the angle is 2-7/16 in. (2.4375 in.) from the top of the angle. The angle is made of ASTM A36 grade steel.

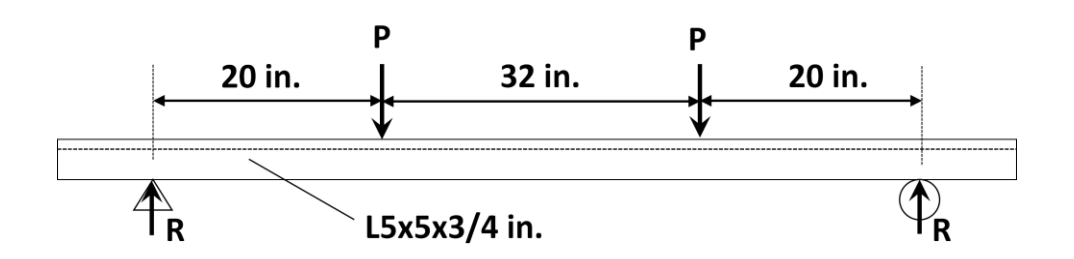


Fig. 20. Load and boundary conditions of laser support platform.

The total weight of laser and the mount, P	= 70 lb (laser) + 60 lb (mount)			
	=130 lb			
Self-weight of the angle (a uniform load), w	= 23.6 lb/ft			
For equilibrium, shear force at support, R	= P + w (6 ft)/2			
Maximum moment at center, M_{max}	$= P \times (32 \text{ in.}) + w (6 \text{ ft})^2/8$			
For the angle with holes,				
1-1/16 in diameter holes for 1 in dia. bolt	= (1 + 1/16) in = 1.0625 in			
Area (cross section with holes)	= (5 in -1.0625 in) × 0.75 in			
	+ (4.25 in – 1.0625 in) × 0.75 in			
= 5.344 in^2 (compared to 6.98 in^2 for the section without holes)				
Neutral axis depth, Y _P	= [3.9375 in × 0.75 in × 0.375 in			
	+ 4.25 in × 0.75 in × 2.875 in			
	-1.0625 in \times 0.75 in \times 2.4375 in]/ 5.344 in 2			
	= 1.559 in			
Second moment of area, I	= 1/12 × (3.9375 in) (0.75 in) ³			
	+ (3.9375 in) (0.75 in) × (1.559 in- 0.375 in) ²			

 $+1/12 \times (0.75 \text{ in}) (4.25 \text{ in})^3$

+ (0.75 in) (4.25 in) (2.875 in -1.559)²

-1/12 (0.75 in) (1.0625 in)³

-(0.75 in) (1.0625 in) (2.4375 in-1.559 in)²

 $=0.1384 \text{ in}^4 + 4.1398 \text{ in}^4 + 4.7979 \text{ in}^4$

+ 5.5203 in⁴ -0.0750 in⁴ -0.6150 in⁴

=13.906 in⁴ (compared to 15.7 in⁴ for solid

Angle without holes, from AISC steel

construction manual)

Moment capacity of the angel with holes = $(\phi \times \sigma_y \times I) / (5 \text{ in. -Yp})$

 $= (0.9) (36 \text{ ksi}) (13.906 \text{ in}^4)/(5 \text{ in}-1.559 \text{ in})$

= 130.9 kip.in

Shear capacity of the 1 in-dia. bolt (A325) = 40 kip (with 0.75 strength reduction favor,

from AISC manual)

Maximum moment, $M_{max} = p \times 32 \text{ in} + (23.6 \text{ lb/ft}) (6 \text{ ft})^2/8 = 130.9 \text{ kip.in}$

 $P = [(130.9 \text{ kip.in}) \times (1000 \text{ lb})/1 \text{ kip})-106.2 \text{ lb.ft } (12\text{in.} /1 \text{ ft})]/32 \text{ in.}$

 $P_{max} = 4051 lb$

For the two angles in one laser platform,

The maximum load $= 2 \times P_{max}$

 $= 2 \times 4051 lb$

= 8102 lb

Weight of the laser and the mount = 70 lb (laser) + 60 lb (mount)

= 130 lbs

Factor of safety = 8102 lb / 130 lb

= 62.3

FOS \cong 60 Ok!

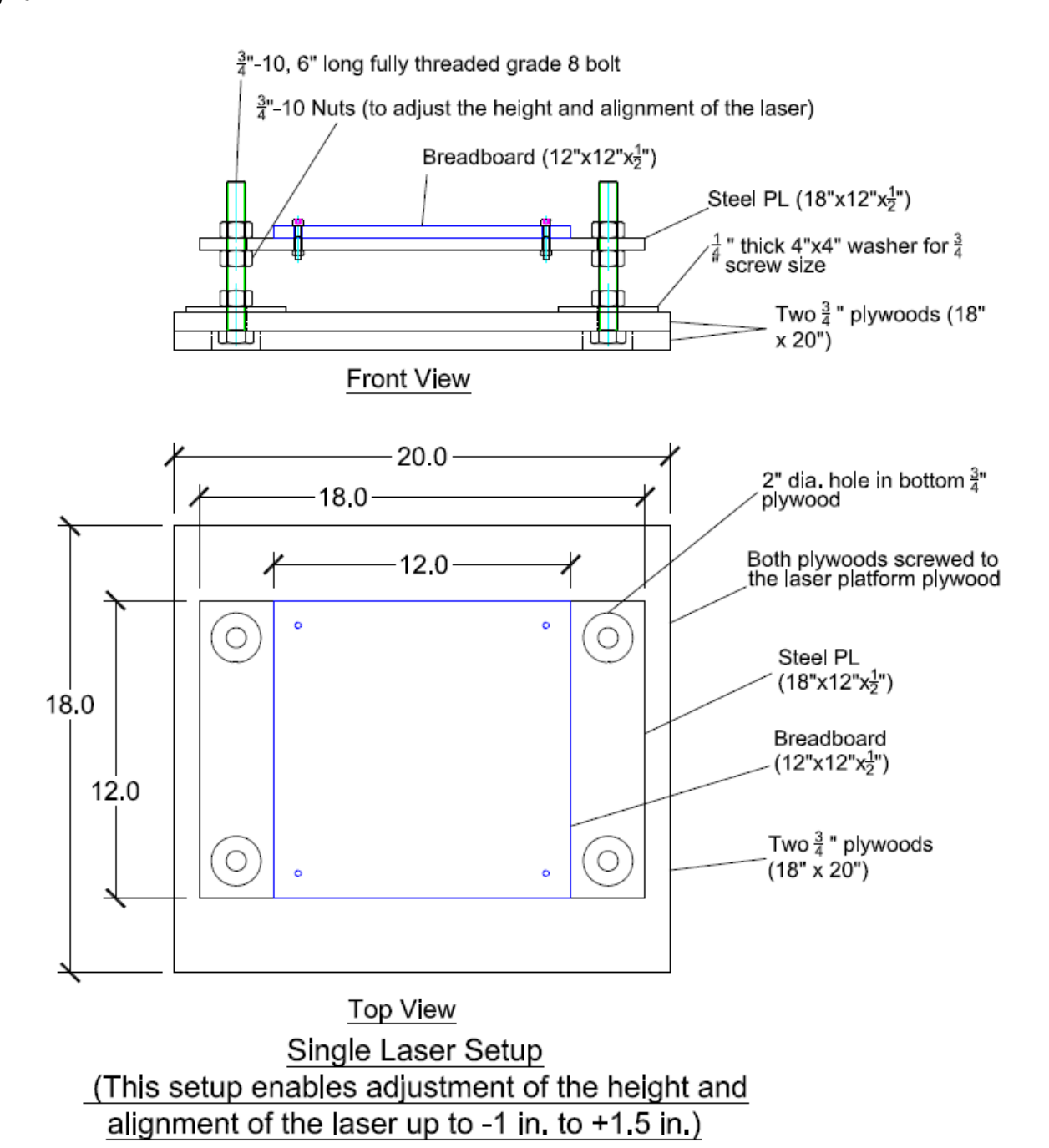


Fig. 21. Elevated platform attachment to the laser instrument setup (dimensions in inches; 1 in. = 2.54 cm).

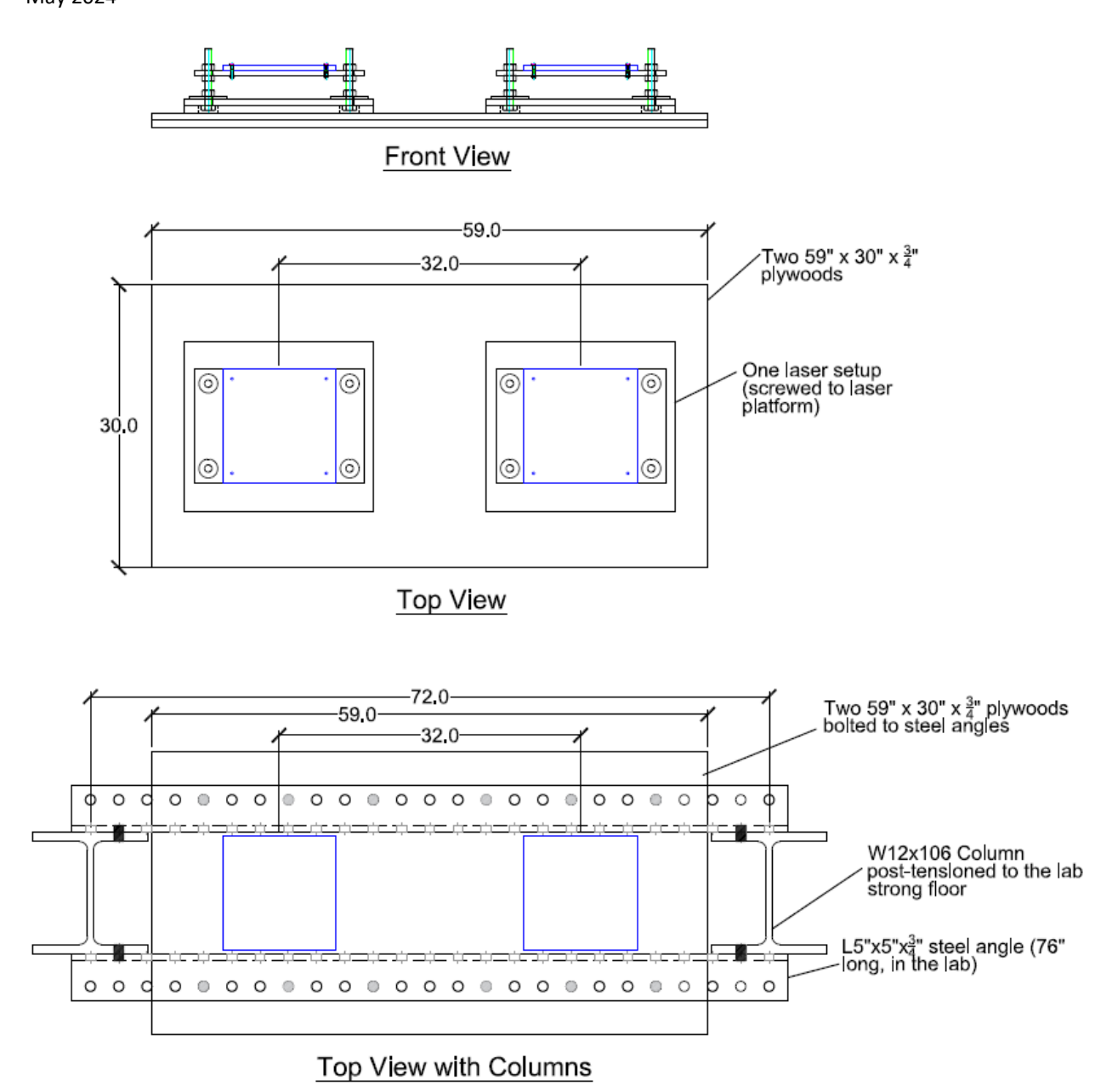


Fig. 22. Elevated platform attachment to the top of the support columns (dimensions in inches; 1 in. = 2.54 cm).

Lasers Attached to Columns

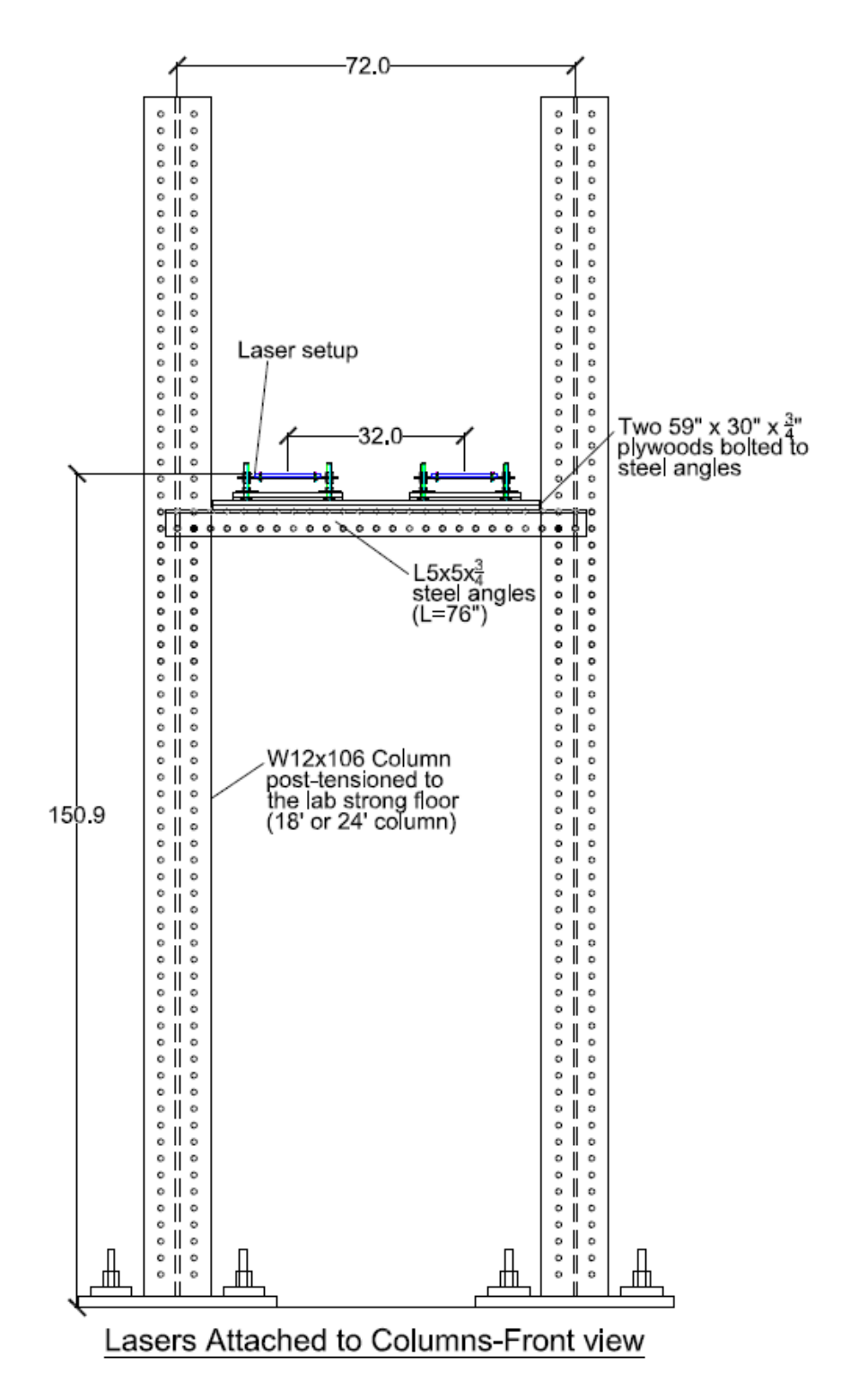


Fig. 23. Elevated platform attachment to the two columns and column attachment to the floor (front view; dimensions in inches; 1 in. = 2.54 cm).

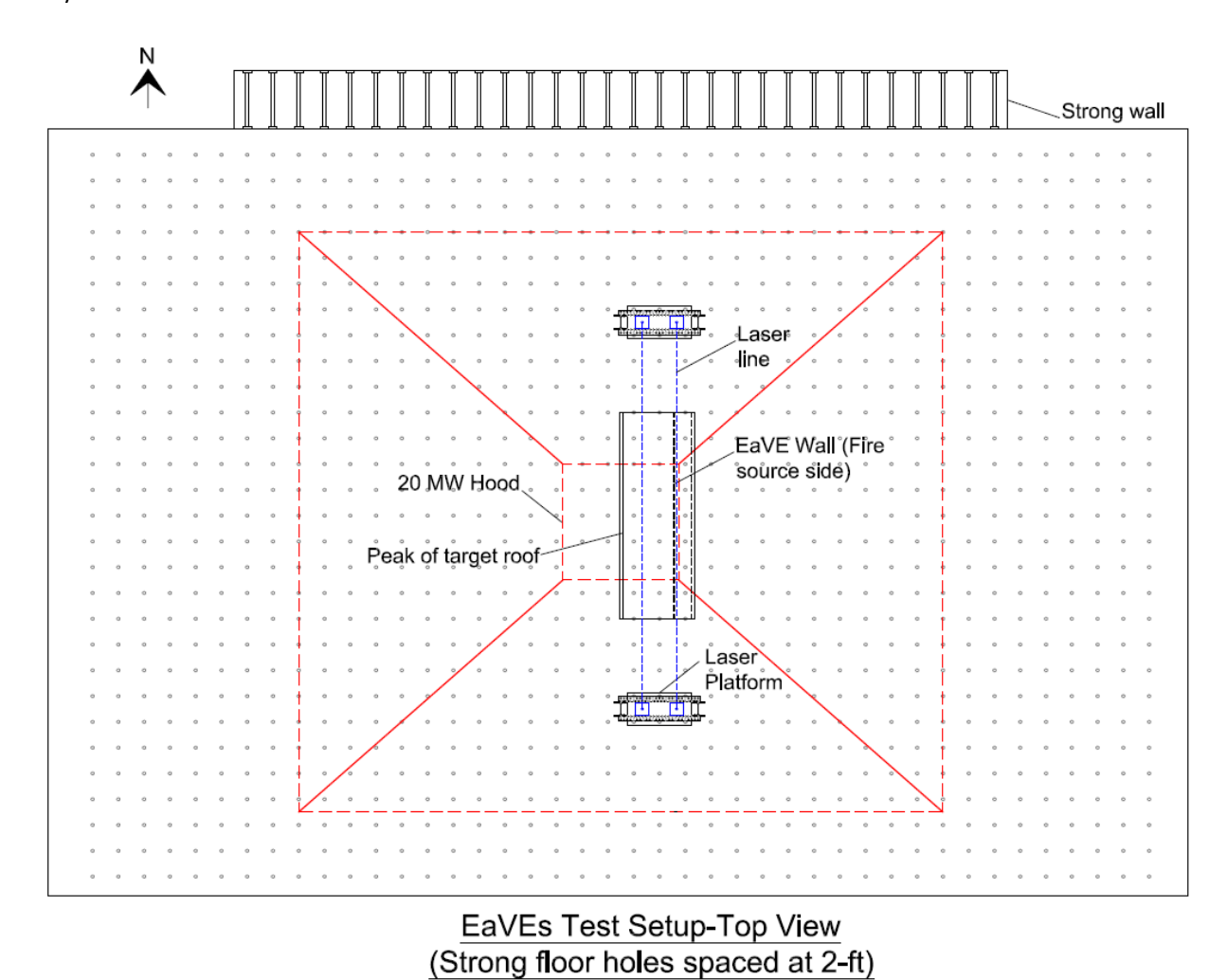


Fig. 24. Top view of the elevated platform and columns to the north and south of the target structure with the roof peak centered under the hood.

Appendix D – Experiment SOP

Safe Operating Procedures:

- 1. Pre-test performed by qualified NFRL Staff
 - a. Prepare and place target structure.
 - b. Place source structure with predetermined fuel (cribs) loading in place.
 - c. Install support structures for elevated platform for laser instruments (see JHA for installing elevated platforms for lasers)
 - d. Install and secure water-cooled heat flux gauges (HFG) at prescribed locations around the target structure.
 - e. Turn on exhaust fans and open makeup air dampers.
 - f. Verify that area CO detectors and alarms are functioning. At least two carbon monoxide alarms must be placed near test personnel before test is initiated.
 - g. Turn on measurement systems and verify that they are functioning.
 - h. Turn on lighting and verify camera settings.
 - i. Notify NIST Fire Department of impending fire tests and deactivate (place in bypass) automatic fire suppression systems.
 - j. Mark exclusion zone along the hood boundary.
 - k. Prepare the ignition source (spark, pilot tube, etc.).
- 2. Ensure water supply to HFGs. Cover and protect back/exposed surfaces of measurement devices and wires using thermal insulation or a radiation shield.
- 3. Verify that all fire suppression water lines are functioning.
- 4. Prepare NFRL data acquisition system to record data.
- 5. Test Director Conducts Safety Briefing and completes safety checklist. (see NFRL Large Fire Experiments 733.06.0132). The Safety Briefing is limited to individuals identified by the Test Director. Personnel who do not attend the safety briefing shall not enter the test area after this point unless authorized by the Safety Officer and briefed on the hazards.
- 6. Verify Absorption Spectroscopy instruments are in place, aligned, and related protection for instrument cables and heat shielding is in place (see EavesAbsorptionSpectroscopy_SOP-ERP_v5b.docx, and Open-Path Absorption Spectroscopy for Eave Vent Monitoring Hazard Review 646.10.0471.122923i).
- 7. Spectroscopy instruments are started.
- 8. Turn on video and IR cameras.
- 9. Start data acquisition.
- 10. Acquire background data for Heat Release Rate (HRR).
- 11. Qualified NFRL staff will ignite the wood cribs within the source structure to start the experiment.
 - a. Check the propane tank and wand assembly for leaks with a flammable gas leak detector.
 - b. If a leak is detected, do not proceed with the activity until the leak is addressed.

- c. Open the tank's valve.
- d. Ignite the flame using the spark igniter. Set the flame length of about 2.5 cm.
- e. Approach the source structure with wood cribs inside.
- f. Apply the flame under the center crib to ignite heptane in aluminum pan.
- g. After ignition, shut off the tank's valve.
- h. Move away from the ignited item and outside the exhaust hood to a safe distance.
- i. In addition to the staff member igniting the item (Staff 1), a second staff member (Staff 2) shall maintain line of sight and audible contact with Staff 1. Both shall be equipped with the required PPE and Fire-resistant lab coat. Staff 2 shall be prepared to assist Staff 1 to safely move away from the ignited item in case of unforeseen events that may affect Staff 1 (slip, trip, fall, etc.).
- 12. Source-Structure-only experiments (no target structure) A number of experiments with sheds and cribs (fuel) will be conducted with no target structure in place until the fuel is completely burned to measure baseline HRR.
- 13. Source Structure with Target Structure experiments At any time, active suppression will be employed to extinguish the fire if the Safety Officer and representative from the project team feel it is safer to do so. All energized instrumentation will be de-energized before active suppression commences.
- 14. End of experiment criteria will be decided by the PI in consultation with the workspace manager. Experiment will end when one of the following occurs:
 - a. Normal end of test criteria Fuel burn out, no fire penetration through the eave vent, temp on unexposed side of vent < 350 °C, target structure does not burn, unless the Test Director, in consultation with the Safety Officer and a representative from the project team, decide to suppress the fire sooner.
 - b. Vent failure Flame penetrates through the eave vent, temp > 350 °C on unexposed side of vent
 - c. Target structure ignites (roof, eaves, or wall) If the target structure ignites, there shall be at least two independent lines of defense for fire suppression:
 - i. First: Suppression by NIST Fire Department (x6190) or trained NFRL staff
 - ii. Last line of defense: Suppression using the NFRL automatic water deluge system, which can be activated manually when the system is in bypass.
- 15. Stop data acquisition, stop cameras, stop spectroscopy.
- 16. Ensure there is no potential for re-ignition of test materials before burned materials are properly secured, stored or discarded.
- 17. Allow debris to cool to ~ 50 °C before safely discarding (see Post Experiment Debris Removal and Repairs for Eave and Vent (EaVE) Experiment FLHR 733.01.0249.111623i)
- 18. NFRL staff safety officer notifies NIST FD of completion of fire tests and re-activates (brings online) automatic fire suppression systems.
- 19. Target wall will be assessed and repaired or reassembled if needed, and eave vent replaced (see Target and Source Assembly for Eave and Vent (EaVE) Experiments

NIST TN 2288 May 2024

733.01.0250.111623i and Post Experiment Debris Removal and Repairs for Eave and Vent (EaVE) Experiments 733.01.0249.111623i)

Appendix E - Modeling Details

Numerical simulations were performed using Fire Dynamics Simulator (FDS) to explore various conditions relevant to the design of our experimental setup. The main objectives of this preliminary simulation campaign were:

- 1. Assessing the influence of open outlets on the rear side of attics and examining how varying the size of these openings affects the dynamics.
- 2. Analyzing whether the presence or absence of an attic affects wind flow and consequent heat exposure, and investigating how the size of the attic may impact overall conditions.
- Establishing a baseline scenario and collecting input data for modeling the laser setup.

A summary of the simulation procedure and results is presented in this section. The simulation setup was designed to analyze the attic's effect on temperature, oxygen fraction concentration, and wind velocity within the attic space, and with particular emphasis on regions beneath the eave. No wind conditions were considered, and the wall structures were treated as inert material. In all cases, the fire was simulated as the ejection of gaseous fuel from a solid surface with an area of 0.25 m² and a constant Heat Release Rate (HRR) of 250 kW/m², located beneath the central bay. Grid cell sizes of 2 cm and 4 cm were evaluated, and all the results presented here were obtained using the finer resolution grid. To optimize computational resources, certain cases assumed the floor to be at the same level as the heat source, as illustrated in Fig. 25. The impact of this approximation was assessed, revealing negligible effects on the simulation results. The different attic sizes assessed in this simulation campaign are outlined in Table 5 and compared with the base case, where no attic exists. In all cases, the dimensions (depth, width, and height) of the attics were determined following the diagram depicted in Fig. 26.

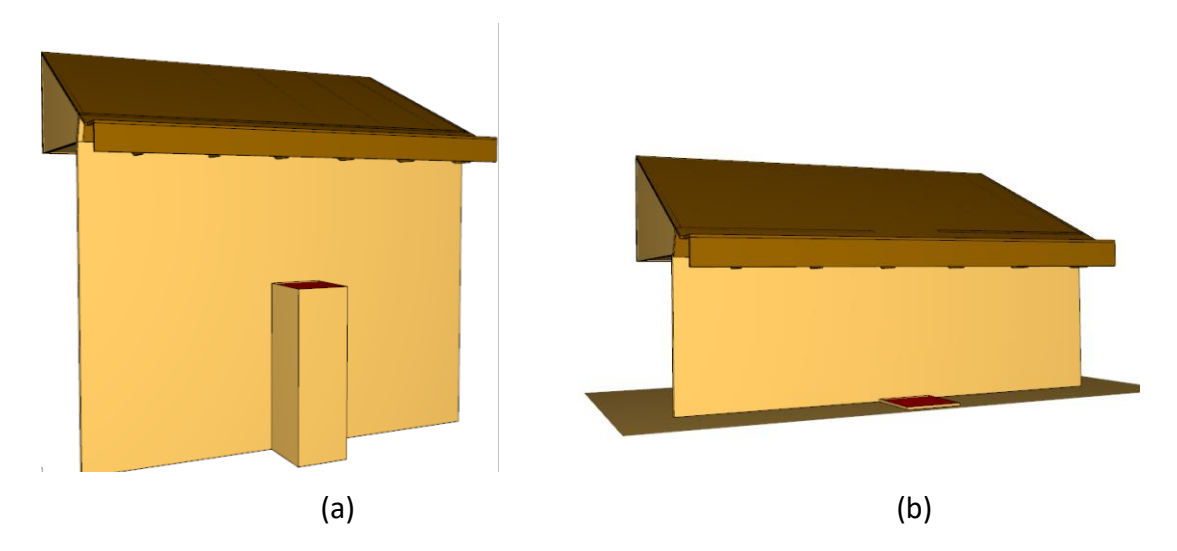


Fig. 25. Simulation set up considering (a) heat source 1.44 m above the floor and (b) heat source at floor level.

Table 5. Simulations cases varying dir	mension in different directions.
--	----------------------------------

Simulation case	Depth (m)	Width (m)	Height (m)	Approximated volume (m³)
SxSSySz	1.6	1.8	0.94	1.36
SxSySz	1.6	2.4	0.94	1.8
SxMySz	1.6	3.4	0.94	2.55
MxSyMz	2.24	2.4	1.2	3.2
MxMyMz	2.24	3.4	1.2	4.6
MxMyLz	2.24	3.4	1.7	6.47

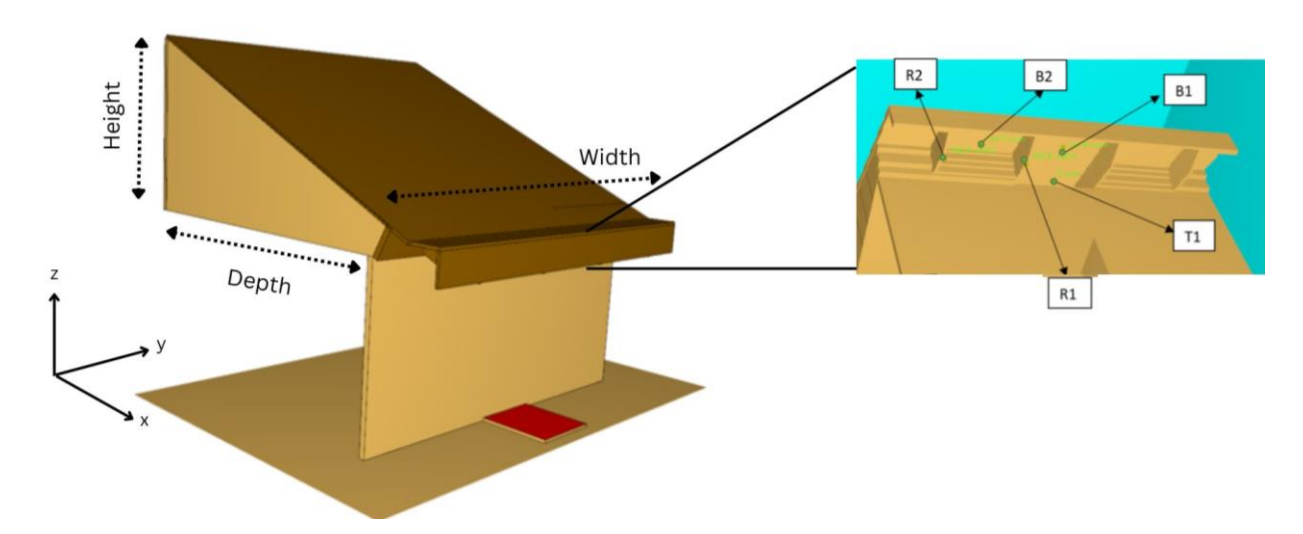
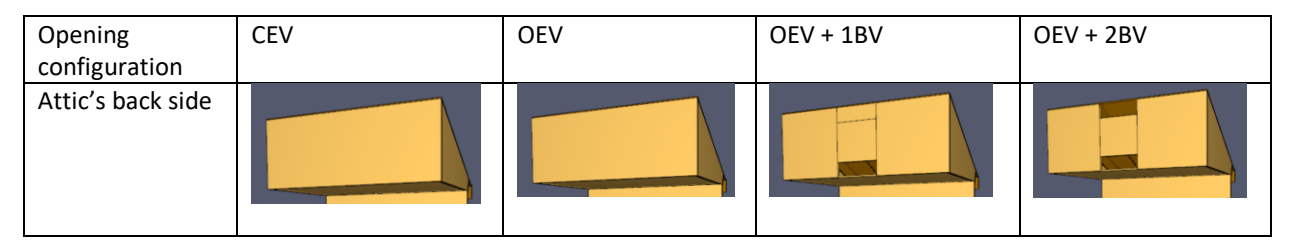


Fig. 26. Location of temperature and oxygen fraction measurements beneath the eave.

Effect of openings on the attic

To evaluate the influence of openings in the attic, serving as both inlets under the eave and inlets or outlets on the backside, mean gas temperature and oxygen fraction were obtained during the simulations. These parameters were calculated in the central bay (B1), the adjacent bay (B2), and within the adjacent rafters (R1 and R2), as illustrated in Fig. 26. For this evaluation, the selected opening configurations are detailed in Table 6. "CEV" represents the scenario where neither an inlet nor an outlet opening is included. "OEV" signifies a configuration where only one eave vent functions as an inlet, positioned beneath the eave area, with no outlet included. "OEV +1BV" and "OEV +2BV" correspond to setups where the eave vent is open, and one or two additional vents, respectively, are situated on the backside of the attic. In the case of a single vent on the backside, it serves as an outlet opening. However, in the "OEV +2BV" scenario, the lower vent functions as an inlet, while the upper one acts as an outlet.

Table 6. Schematic of the attic rear for each tested opening configuration.



As an example of the effect of the opening configuration in the overall fire dynamics, simulation results for the case SxSySz are presented as a function of the type of opening configuration in Fig. 27. Shadow bars highlight the standard deviation of the opening configuration "OEV+1BV" data. In the cases evaluated during this study, a consistent trend was observed across different attic sizes: a decrease in temperature in the rafters and adjacent bay as the number of outlet openings increased. This phenomenon can be attributed to the increasing influx of cold air through the vent, driven by the suction effect of the outlet openings. The simulations revealed that the mean average wind speed increases within the plume when outlets are added, and since the opening area of the eave vent remains constant, a higher flow rate through the vent is generated. This results in more cold air being drawn from the surroundings. As a result, the adjacent areas to the fire plume experience a cooling effect.

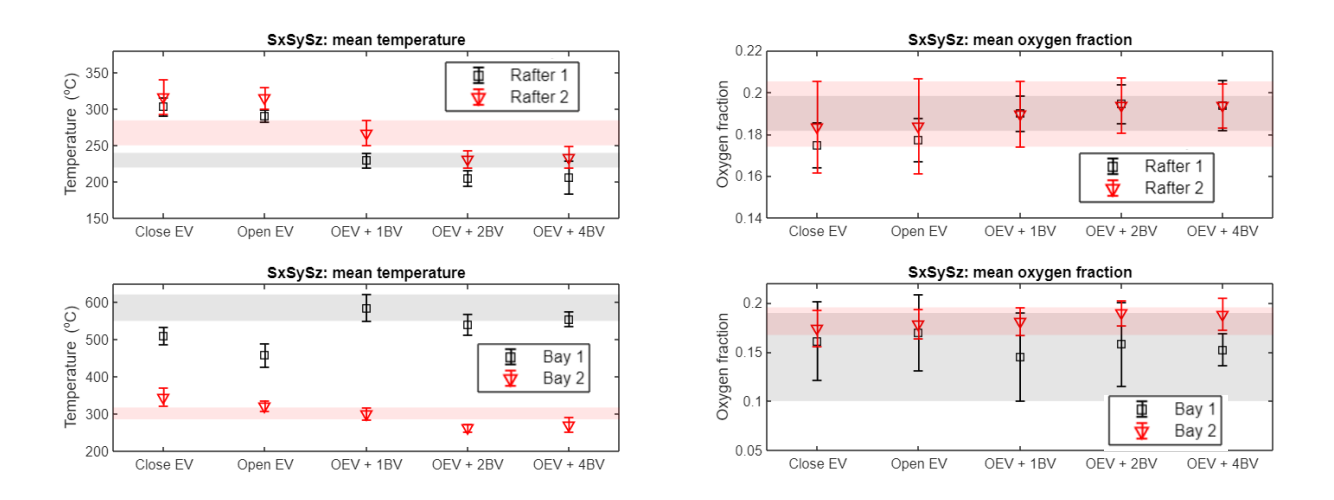


Fig. 27. Mean temperature and oxygen fraction for various opening configurations for simulation case SxSySz.

When comparing these previous results with those obtained for a larger attic size, most cases do not exhibit significant difference (~ 5%). The only notable variation was observed in the temperature of the central bay. For instance, when comparing the average temperature for cases SxSySz and SxMySz under the "CEV" configuration, the larger attic size case displayed approximately a 15 % lower temperature. A similar effect was observed for the "OEV" configuration. However, for the remaining opening configurations, no significant differences were found.

Impact of the attic

To determine the optimal location for the open-path laser spectrometer and establish a baseline for gas-phase concentration and temperature measurements in both the eave and attic spaces of the target wall structure, average volume oxygen concentrations were obtained for various simulation setups. These measurements were conducted throughout the attic and eave areas, as illustrated in Fig. 28. In addition to the simulation cases outlined in Table 5, a wall target with dimensions matching case SxSSySz but without an attic was included. This was done to evaluate the attic's impact on these parameters, some of which will be discussed later.



Fig. 28. Volume location where averaged oxygen fraction was computed during the simulations.

The time histories of volume-averaged oxygen fractions at both locations for some of the simulation cases are shown in Fig. 29. These results were used as input data for modeling the laser setup. The most significant disparity in mean values during the quasi-steady state across the eave was observed between the largest attic case (MxLyLz) and the smallest one (SxSSySz), with the former exhibiting a mean oxygen fraction approximately 6 % higher across the eave. Conversely, for oxygen fraction inside the attic, the oxygen levels decrease over time, and the attic's size primarily determines how long it takes for the configuration to reach the minimum value of oxygen fraction available within the attic, as illustrated in Fig. 29(b). Furthermore, the mean temperatures in the bays and rafters for various simulation cases are presented in Table 7 showing no statistical difference for most of the cases.

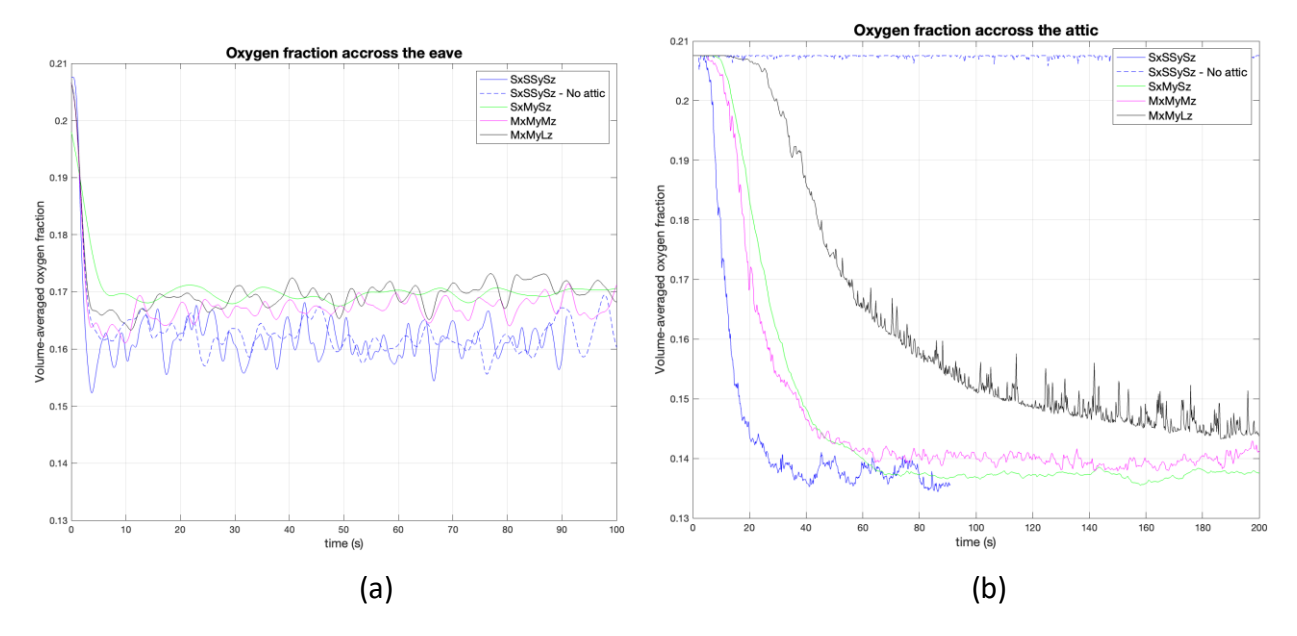


Fig. 29. Time histories of volume-averaged oxygen fractions across (a) the eave area and (b) the attic.

Table 7. Mean temperature in the central bay (B1), the adjacent bay (B2), and within the adjacent rafters (R1 and R2). Standard deviation is indicated within parentheses.

	Mean temperature (°C)			
Simulation case	B1	R1	B2	R2
SxSySz	520 (150)	216 (10)	236 (9)	268 (12)
SxSySz – no attic	490 (142)	210 (13)	232 (11)	258 (13)
SxMySz	495 (64)	227 (10)	250 (9)	280 (10)
MxMyMz	485 (112)	219 (14)	240 (14)	270 (16)
MzLyLz	407 (120)	202 (7)	225 (11)	257 (12)

As a part of the analysis of the attic's impact on overall dynamics, a comparison was made between simulation cases with and without an attic. In addition to the results presented in Fig. 29, which showed minimal impact of the attic on oxygen fraction, with only a 1 % increase compared to cases without an attic, wind speed and gas temperature were measured 2 cm inside the eave vent opening. Results for the simulation case SxSySz are presented in Fig. 30, indicating no significant effect on gas temperature at these locations. However, a ~17 % higher wind speed was observed for the case without an attic compared to the case with an attic. This suggests that the back pressure established by the presence of the attic could influence wind flow through the opening. Therefore, it is crucial to evaluate this value during future experiments to gain insight into this effect and provide a baseline for validating future simulations.

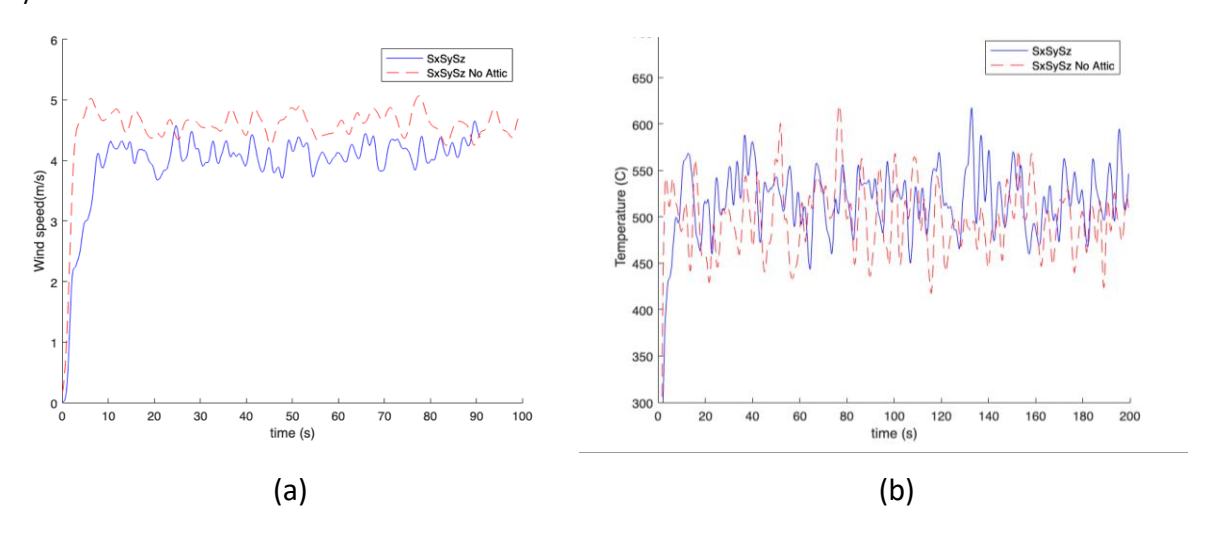


Fig. 30. Result for the simulation case SxSySz with and without attic, (a) wind speed and (b) gas temperature, both measured 2 cm inside the eave vent opening.

Summary

The previous results aim to provide guidance for experimental design. However, it's important to consider the limitations. Since this was a preliminary simulation campaign, simplifications were made to the experimental setup, such as only considering a constant heat source. Therefore, some of the impacts on the variables reported here may be influenced by changes to this source. However, these simulations serve as a base case to provide insights into fire dynamics details that were not observable during experiments.

Key conclusions from the simulations include:

- 1. A consistent decrease in temperature beneath the eave was observed as the number of outlets increased across various attic sizes.
- 2. The size and presence of the attic do not seem to significantly affect temperature, but they do have some impact on oxygen fraction. Inside the attic, the size primarily determines the time it takes for the configuration to reach the minimum available oxygen fraction, while beneath the eave, there was minimal impact on oxygen concentration.
- 3. The most significant impact of the attic's presence was on wind speed, with a 17 % higher wind speed observed for the case without an attic compared to the case with an attic.

These findings provide a starting point for future model validation by incorporating experimental results from future experiments.